NASA TECHNICAL NOTE

NASA TN D-6348

NASA TN D-6348

COMPARISON OF WIND-TUNNEL AND FLIGHT-MEASURED BASE PRESSURES FROM THE SHARP-LEADING-EDGE UPPER VERTICAL FIN OF THE X-15 AIRPLANE FOR TURBULENT FLOW AT MACH NUMBERS FROM 1.5 TO 5.0

by Sheryll A. Goecke

Flight Research Center
Edwards, Calif. 93523

NATIONAL AERONAUTICS AND SPACE ADMINISTRATION • WASHINGTON, D. C. • MAY 1971

1. Report No.	2. Government Accession No.	3. Recipient's Catalog No.
NASA TN D-6348		

4. Title and Subtitle	5. Report Date
COMPARISON OF WIND-TUNNEL AND FLIGHT-MEASURED BASE PRESSURES FROM THE SHARP-LEADING-EDGE UPPER VERTICAL FIN OF THE X-15 AIRPLANE FOR TURBULENT FLOW AT MACH NUMBERS FROM 1.5 TO 5.0	May 1971
	6. Performing Organization Code

7. Author(s)	8. Performing Organization Report No.
Sheryll A. Goecke	H-602
	10. Work Unit No.
9. Performing Organization Name and Address	722-51-00-01-24
NASA Flight Research Center P. O. Box 273 Edwards, California 93523	11. Contract or Grant No.
	13. Type of Report and Period Covered
12. Sponsoring Agency Name and Address	Technical Note
National Aeronautics and Space Administration Washington, D. C. 20546	14. Sponsoring Agency Code

15. Supplementary Notes

16. Abstract

Pressures measured at six locations on the base of the sharp-leading-edge upper vertical fin of the X-15 airplane during the power-off portion of eight flights are compared with previous flight data obtained from a blunt-leading-edge fin, theory, and wind-tunnel data. The flight and wind-tunnel base pressure ratios for the Mach number range from 1.5 to 5.0 are presented as a linearized function of turbulent boundary-layer height and base width by using a Mach-number-dependent factor derived in the study. The resulting curve seems to provide another criterion for determining whether flow is laminar or turbulent. The difference between base pressure and free-stream pressure for any specific Mach number of the study is found to be a linear function of both free-stream pressure and dynamic pressure. Data from the sharp-leading-edge upper vertical fin agree with data from the blunt-leading-edge upper vertical fin. The flight data show the variation in pressure across the base to be negligible.

17. Key Words (Suggested by Author(s))	18. Distribution Statement
X-15 airplane - Base pressure - Drag - Separated flow	Unclassified - Unlimited

19. Security Classif. (of this report)	20. Security Classif. (of this page)	21. No. of Pages	22. Price*
Unclassified	Unclassified	38	$3.00

*For sale by the National Technical Information Service, Springfield, Virginia 22151

COMPARISON OF WIND-TUNNEL AND FLIGHT-MEASURED BASE PRESSURES FROM THE SHARP-LEADING-EDGE UPPER VERTICAL FIN OF THE X-15 AIRPLANE FOR TURBULENT FLOW AT MACH NUMBERS FROM 1.5 TO 5.0

Sheryll A. Goecke
Flight Research Center

INTRODUCTION

Because base drag can be a substantial amount of the total drag of an aircraft, the local pressure on blunt bases formed by the trailing edges of wings and control surfaces, abrupt changes in contour, or resulting from propulsion installations after engine shutdown has been of interest for many years. Theoretical and semiempirical studies as well as wind-tunnel investigations have provided methods of predicting base pressures at moderate Reynolds numbers for various simple, two-dimensional shapes (refs. 1 to 5). Some base pressure data have been obtained from full-scale airplanes, for example, on the X-15 airplane for Mach numbers from 1.1 to 3.2 (ref. 6) and up to 6 (ref. 7).

This report presents flight base pressure data for turbulent flow obtained from the base of the sharp-leading-edge upper vertical fin of the X-15 airplane. (The leading edge was blunt for the studies of references 6 and 7.) A representative base pressure was assured by taking measurements at six locations, three along the centerline and three near the edges (to within about 3 percent of the mean base thickness from the edge). The sharp leading edge and the assurance of a representative base pressure from the base, as well as the subsequent availability of wind-tunnel data for conditions similar to flight conditions, permitted a more comprehensive comparison between flight and wind-tunnel data than was possible in previous X-15 base pressure reports. Because base pressure data are often obtained for discrete Mach numbers and for certain ratios of boundary-layer momentum thickness to base width, comparing data from different experiments can be difficult. The wind-tunnel data of reference 2 and the flight data of the present study and of reference 7 are used in developing a method for comparing the base pressure ratio as a function of turbulent boundary-layer height, base width, and Reynolds number for the Mach number range of 1.5 to 5.0. In addition, the method is examined as a possible criterion for observing whether the flow is laminar or turbulent.

The data of this study and of reference 7 are compared to determine the significance of the inviscid blunt-leading-edge effects of reference 7 when the diameter of the leading edge is about 1 percent of the chord. The data are for free-stream Mach numbers between 1.5 and 5.0 and were obtained during the power-off, or glide, portion of eight X-15 flights.

SYMBOLS

Physical quantities in this report are given in the International System of Units (SI) and parenthetically in U. S. Customary Units. The measurements were taken in U. S. Customary Units. Factors relating the two systems are presented in reference 8.

B	a constant (see appendix)
$C_{p,b}$	base pressure coefficient, $\frac{p_b - p}{0.7M^2p}$
c	chord length, m (ft)
d	diameter of leading edge of vertical fin, cm (in.)
h	width of base of fin or airfoil (equivalent step height is h/2), cm (in.)
k	Mach-number-dependent value from reference 4
k_1	Mach-number-dependent value (see appendix)
M	free-stream Mach number
N_{Re}	Reynolds number, $\frac{\rho V}{\mu} c$
p	free-stream static pressure, N/cm^2 or N/m^2 ($lb/in.^2$ or lb/ft^2)
p_b	base static pressure, N/cm^2 or N/m^2 ($lb/in.^2$ or lb/ft^2)
q	dynamic pressure, $0.7M^2p$, N/m^2 (lb/ft^2)
s	standard deviation
V	free-stream velocity, m/sec (ft/sec)
$\Delta(p_b/p)$	data band

δ average deviation

θ momentum thickness, cm (in.)

μ absolute viscosity, kg/m-sec (lb/ft-sec)

ρ density, kg/m^3 (lb/ft^3)

AIRPLANE AND TEST CONFIGURATION

Airplane

The X-15 airplane was a single-place, low-aspect-ratio, hypersonic, rocket research vehicle (fig. 1) with a design Mach number of 6. The major physical characteristics of the airplane are presented in table 1. The X-15 airplane was launched from a modified B-52 bomber at an altitude of about 13.7 kilometers (45,000 feet) and a Mach number of approximately 0.8. After the powered portion of the flight was completed, the airplane glided to a landing on the dry lakebed at Edwards, Calif. Maximum velocity and altitude obtained during the flight program, by a modified X-15 airplane[1], were 7273 kilometers/hour (4520 miles/hour) and 108.0 kilometers (354,200 feet), respectively.

Test Configuration

A side view of the movable portion of the upper vertical fin, referred to hereafter for convenience as the fin, is shown in figure 2. A closeup view of the base region (an enlargement of the base region of figure 2) and the locations of the six pressure orifices (referred to as taps) are shown in figure 3(a). The base surface was recessed and was corrugated. The depth of the recess from the outer edge to the base surface depended on the corrugation and varied from 0.71 centimeter (0.28 inch) to 1.67 centimeters (0.66 inch).

The base pressure data in references 6 and 7, as previously mentioned, were obtained from a fin with a blunt leading edge (d = 2.54 centimeters (1.0 inch)) with a c/d ratio of approximately 100. For the present study the upper three-fourths of the fin leading edge was modified to a diameter of 0.076 centimeter (0.03 inch) with a c/d ratio of approximately 3500. On the bottom fourth of the fin, the leading-edge diameter changed from the sharp-leading-edge diameter to the blunt-leading-edge diameter of the stationary portion of the fin (fig. 3(b)). Taps A to E were downstream of the sharp-leading-edge portion, and tap F was downstream of the changing diameter and, hence, the blunter portion of the leading edge. The three taps along the centerline of

[1]The fuselage was lengthened; external, jettisonable tanks were added; and the airplane was coated with an ablative.

the base were at essentially the same locations as three of the four taps in the blunt-leading-edge study of reference 7. Two of the three taps near the edges, D and E, were moved closer to the edge for some of the flights.

Boundary-layer trips from a previous experiment were located on the right side, 12.20 centimeters (4.8 inches) back from the leading edge of the sharp-leading-edge fin. Approximately 15 centimeters (6 inches) back from the leading edge on both sides of the fin, raised screw heads and a gap between the leading-edge surface and the rest of the fin caused surface roughness.

Detailed dimensions and photographs of both fin configurations are presented in table 2.

INSTRUMENTATION

Base pressures were recorded by an aneroid type of pressure cell mounted in a standard NACA 12-cell photo-recording manometer. Free-stream Mach number, dynamic pressure, altitude, and free-stream velocity were obtained from a combination of onboard sensor, meteorological, and radar data. Reference 9 discusses how the data were obtained and analyzed. Other flight information needed to monitor such factors as altitudes and control-surface deflections and rates was recorded on NASA flight-recording instruments. All records were synchronized by a common timer.

ACCURACY

The error in base pressure coefficient depends primarily on the errors in free-stream Mach number, free-stream static pressure, and base pressure. Errors in free-stream Mach number and free-stream static pressure were obtained from reference 9. These limit errors, which apply for all the conditions of the study, were ±0.05 for the free-stream Mach number and ±287 newtons/meter^2 (±6 pounds/foot^2) for the free-stream static pressure. The maximum error in base pressure was determined to be ±192 newtons/meter^2 (±4 pounds/foot^2).

The standard deviation, $sC_{p,b}$, resulting from these errors can be found by using the following relationship from reference 10:

$$sC_{p,b} = 1.25\delta C_{p,b}$$

where $\delta C_{p,b}$ is the average deviation derived from equation (37) of reference 10,

$$\delta C_{p,b} = \sqrt{\left(\frac{\partial C_{p,b}}{\partial M}\right)^2 (\delta M)^2 + \left(\frac{\partial C_{p,b}}{\partial p}\right)^2 (\delta p)^2 + \left(\frac{\partial C_{p,b}}{\partial p_b}\right)^2 (\delta p_b)^2}$$

The partial derivatives are obtained from the expression

$$C_{p,b} = \frac{p_b - p}{0.7M^2 p} = \frac{p_b - p}{q}$$

After substituting for the partial derivatives and simplifying, the equation for the standard deviation becomes

$$sC_{p,b} = 1.25\sqrt{\frac{(\delta p_b)^2 + (-p_b/p)^2 (\delta p)^2}{q^2} + (-2C_{p,b})^2 (\delta M)^2}$$

Dynamic pressure, q, was not constant for a given Mach number; therefore, the standard deviation in the following table represents a maximum value obtained by using the smallest value of dynamic pressure at a specific Mach number:

M	$sC_{p,b}$	Limit, percent, $\frac{sC_{p,b}}{C_{p,b}}$	Faired, percent, $\frac{sC_{p,b}}{C_{p,b}}$
1.5	±0.052	±15	±5
3.0	±.019	±15	±5
5.0	±.015	±30	±10

Because the individual source errors can vary at random in both sign and magnitude within their limits, the errors will tend to cancel one another. Therefore, the deviations from the main body of data are smaller than predicted by the $sC_{p,b}$. The average value of $C_{p,b}$ derived from fairing through the data in figure 4 is believed to be within the values shown in the last column.

Lag was determined by observing the time required for the base pressure system to sense that the airplane's rocket engine had shut down. The maximum lag observed was 1 second; most of the data had less than one-half second of lag.

TEST CONDITIONS

The base pressure data presented in this report were obtained during the power-off, and, hence, decreasing free-stream Mach number, portion of eight flights. The free-stream Mach number, hereafter referred to as Mach number, ranged from 1.5 to 5.0. Altitude and dynamic pressure varied from 13.4 kilometers (43,900 feet) to 36.5 kilometers (119,700 feet) and 0.862 newton/centimeter^2 (180 pounds/foot^2) to 5.75 newtons/centimeter^2 (1200 pounds/foot^2), respectively.

Reynolds number, based on the mean chord of the fin of 2.7 meters (8.8 feet), ranged from 3.83×10^6 to 21.40×10^6. This high Reynolds number, together with the trips and roughness mentioned in the Test Configuration section, indicates that turbulent

flow should begin relatively close to the leading edge of the fin. Turbulent flow was verified near the leading edge on this fin to a local Mach number of 4.9 (ref. 11) for the same leading-edge roughness. Thus, for the conditions of this study, turbulent flow was considered to exist for a mean length of 2.56 meters (8.4 feet).

The flow field on the sides of the upper vertical fin for the sharp leading edge and the blunt leading edge was discussed in reference 12. The blunt leading edge showed variation in the flow field in terms of the inviscid-layer stagnation-pressure distribution in both the chordwise and spanwise directions; however, the sharp leading edge had essentially no flow-field variation in either the chordwise or spanwise directions for this parameter. Therefore, the base pressure data in this paper, which are for the sharp leading edge, are essentially in a constant spanwise and chordwise flow field.

The angle of sideslip and angle of attack, neither of which affected the data, varied from ±4° and -2° to 21°, respectively. Speed-brake positions, which varied from closed to partially or fully extended, are indicated, when pertinent, in the figures.

Because the data were obtained after the rocket engine shut down, there were no jet-exhaust effects. Furthermore, there was no base bleed, either planned as part of the experiment or occurring accidentally.

The upper vertical fin, which had a thin boundary layer with respect to the base width, had a ratio of θ/h of approximately [a]0.006 throughout the Mach number range.

RESULTS AND DISCUSSION

Basic Data

The base pressure for any given configuration is usually considered to be a function of angle of attack, angle of sideslip, Mach number, free-stream static pressure, and Reynolds number. As previously stated, in this study the base pressure showed no dependence on either angle of attack or sideslip, but was affected by Mach number, free-stream static pressure, and Reynolds number.

The base pressure coefficient for each location as a function of Mach number is presented in figures 4(a) to 4(f). The three speed-brake positions (closed, opened from 9° to 15°, and opened from greater than 15° to the maximum opening of 36°) are indicated in the figures. The flagged symbols in figures 4(d) and 4(e) represent data obtained after taps D and E were moved closer to the edge of the fin (fig. 3(b)). The data have about the same value for each location for the higher Mach numbers regardless of speed-brake position. For the lower Mach numbers (beginning at 3.5 to 2.5, depending on the tap location), the speed-brakes-closed condition (the more two-dimensional configuration) provides more positive pressure coefficients for all the tap locations. Changing the positions of taps D and E to within approximately 1.27 centimeters (0.50 inch) of the edge had no definable effect on the local pressure coefficients.

---

[a]This value is obtained from the relationship $\theta/h = \frac{ck}{hN_{Re}^{1/5}}$ in which the variation of k with Mach number is obtained from reference 4.

The base pressure coefficients for all locations for two typical flights are compared in figures 5(a) and 5(b). The pressure variation across the base is small, and hence, for most practical purposes, the base pressure for this surface could be adequately defined from one location. Because the data are plotted for individual flights, the flight and configuration conditions are the same for each set of points for a specific Mach number. Hence, only tap location effects and instrument accuracy limitations could cause the small data spread. The data spread at the lower Mach numbers appears to be larger than at the higher Mach numbers, but, because the base pressure coefficient decreases numerically with increasing Mach number, the spread in terms of percent of average-pressure-coefficient level changes little. Thus, in terms of the total base drag of the fin, the differences in local pressure coefficients are negligible, even though the taps closest to the edge of the base were within 3 percent of the base width from the edge.

Average values of the centerline base pressure coefficients for the speed-brakes-closed condition are compared in figure 6 with the blunt-leading-edge data of reference 7 for the same general locations. The data are in good agreement; in fact, the slight differences are negligible when the resulting base drag is considered. This good agreement shows that the inviscid effects of a blunt leading edge appear to have no influence when the c/d ratio is approximately 100 or larger. The data presented in references 2 and 4 also indicated that the base pressure is insensitive to moderate forebody changes.

The turbulent flow Reynolds number based on the mean chord of the fin is on the order of 10^7 for these flight results. This Reynolds number is an order of magnitude larger than the values obtained in most wind-tunnel experiments (refs. 2, 5, and 13 to 15) covering a comparable Mach number range (fig. 7).

Comparison of Flight Data With Theoretical and Wind-Tunnel Results

Base pressure coefficient. – Figures 8(a) to 8(c) compare an average flight base pressure coefficient with theoretical and wind-tunnel results. The flight values of the present study, which were averaged for the six tap locations of each flight and segregated according to speed-brake position (closed or opened) for a specific Mach number, are shown as curves. Above $M = 3.5$, the curves converge.

In figure 8(a), Korst's thin-boundary-layer theory agrees satisfactorily with the flight speed-brake-closed data at the lower Mach numbers and with the combined curve at the higher Mach numbers. (As previously mentioned, the θ/h ratio of approximately 0.006 for the present study represents a relatively thin boundary layer.) The hypersonic approximation, $-1/M^2$, and the zero-base-pressure curves bracket the flight data at the higher Mach numbers.

In figure 8(b), the largest base-width wind-tunnel data of reference 2 agree better with the flight results than do the smallest base-width data. More important, however, is the trend shown by the reference 2 data of more negative base pressure coefficients as the width of the base increases (c/h decreases). This same trend is shown in the flight speed-brakes-closed and speed-brakes-opened data.[1] This is what is expected

[1] Opening the speed brakes resulted in a greater base thickness immediately adjacent to the fin and, hence, a larger effective h for the entire fin (smaller c/h).

according to the viscous-effect criteria of references 2 and 3, which show a direct dependence of the base pressure ratio, p_b/p, upon the ratio θ/h. This relationship qualitatively supports the trend of more negative pressure coefficients for decreasing θ/h ratios in the data of both the present study and reference 2 as the values of c/h (or the effective value of c/h) change and cause a corresponding change in θ/h.

One of the most consistent characteristics of the X-15 base pressure was the tendency of the various base elements to influence one another. In reference 7 it was noted that the influence of the exhaust jet was approximately the same over the top part of the fin as near the jet, and reference 16 showed evidence that the sting effect on the X-15 model may have had a widespread influence[1]. It is believed that the explanation concerning a lower effective θ/h in the preceding paragraph shows that opening the speed brakes caused the pressure coefficient on the adjacent vertical fin to become more negative, thus representing another example of communication between nearby base elements.

The evidence of a sting support effect (ref. 16) was derived by comparing X-15 flight vertical-fin data and corresponding model data. These model fin data are compared in coefficient form with flight data in figure 8(b). The apparent sting effect results in 8 to 15 percent less drag for the model fin (and a less negative pressure coefficient) than obtained from the airplane fin.

Figure 8(c) compares the flight data of the present study with recent wind-tunnel data. All the wind-tunnel data, except the smaller-step-height data of reference 5, have c/h values near the X-15 flight value. As previously discussed, the effective value of h would be larger for the speed-brakes-opened data than for the speed-brakes-closed data. This would then result in a lower c/h value for the speed-brakes-opened data. The trend of a more negative base pressure coefficient as c/h decreases is shown in the data of references 5 and 15 as well as in the flight data.

The changing value of the base pressure coefficient with changes in either θ/h or c/h indicates that the base pressure coefficient is dependent on both momentum thickness and base width. However, this type of presentation does not directly consider the influence of boundary-layer height or base width. The effect of these variables can be seen more clearly when the base pressure ratio is considered as a function of Reynolds number.

Base pressure ratio. – Reynolds number is known to have a determining influence on whether flow is laminar, transitional, or turbulent, and, consequently, on boundary-layer height. In view of the previous discussion about the relationship of base pressure to momentum thickness, the correlation of base pressure parameters with Reynolds number should be considered. In references 14 and 15, data were obtained for a large enough Reynolds number range that the influence of the flow regions (or type of flow) on base pressure ratio (figs. 9(a) to 9(c)) could be observed. The average base-pressure-ratio data for the X-15 airplane with speed brakes opened and closed are well within the turbulent region. The data from other sources (refs. 2, 5, and 13 to 15) are mainly

[1]This apparent sting effect would represent an interference propagated at least 1 sting diameter laterally and one-half sting diameter forward of the sting-model intercept.

in the regions representing transition near reattachment or between separation and reattachment, according to the criteria of reference 15.

Because the X-15 fin data are for turbulent flow, the average base pressure ratio is presented in figure 10 as a function of $\frac{c}{hN_{Re}^{1/5}}$ which is proportional to the ratio of turbulent boundary-layer thickness to base width, h, through the 1/7-power law (ref. 17). Chapman et al. (ref. 2) documented the dependency of base pressure ratio on $\frac{c}{hN_{Re}^{1/5}}$ for Mach numbers of 1.5, 2.0, and 3.10; therefore, the flight data from the present study are compared with the wind-tunnel data of references 2, 5, 13, and 14 and the flight data of reference 7 for similar Mach numbers. At $M \approx 1.5$ and 2.0 the flight data and most of the wind-tunnel data continue, in general, the trend shown by the data of reference 2. For $M = 3.10$, the flight and wind-tunnel data also continue the trend of reference 2 for the thinner boundary layers, $\frac{c}{hN_{Re}^{1/5}} < 0.5$; however, for the larger $\frac{c}{hN_{Re}^{1/5}}$ values, references 5 and 7 have higher and lower base pressure ratios, respectively, than the reference 2 data. In fact, the $h/2 = 0.51$ centimeter (0.2 inch) data of reference 5 for $M = 3.10$ have a value corresponding to the curve for $M = 2.00$. These disagreements at $M = 3.10$ indicate the possibility of changes in flow-field conditions for small step heights (ref. 5) and small base widths (ref. 2) in thin boundary layers and small base widths (ref. [a]7) in thicker boundary layers. In reference 7, a possible explanation given for the difference at $M = 3.10$ was that expansion waves originating over the side fairing subsequently affected the flow ahead of the wing. However, unpublished data from flights of the XB-70 airplane indicate that the base pressure ratio for a small step (approximately 1.3 centimeters (0.5 inch)) in a thick boundary layer is lower at the higher $\frac{c}{hN_{Re}^{1/5}}$ values than expected on the basis of the curves of reference 2. The results from the use of Korst's thin-boundary-layer theory (ref. 1) are shown as solid symbols.

It is evident from figures 9(a) to 9(c) and figure 10 that comparisons can be made only for specific Mach numbers, i.e., each correlating curve is valid for a narrow range of Mach numbers. Because it is not always easy to obtain flight and wind-tunnel data at a particular Mach number, the curves of figures 9(a) to 9(c) and 10 represent a limited amount of data, even though they cover a range of Reynolds numbers or c/h values. A more general method of determining both the type of boundary-layer flow and the trend of the data for that flow for a range of Mach numbers would be desirable.

---

[a]The data for high values of $\frac{c}{hN_{Re}^{1/5}}$ were obtained from the trailing edge of the X-15 wing (c = 277 cm (109 in.)). Therefore, the boundary layer is substantially thicker than in either reference 2 or 5.

By using the wind-tunnel data of reference 2 and flight data from the present study and reference 7, a Mach-number-dependent factor k_1 was devised (see appendix) so that the base pressure ratio could be presented (fig. 11) as a linearized function of $\frac{c}{k_1 h N_{Re}^{1/5}}$ for Mach numbers from 1.5 to 5.0 instead of only at the most studied Mach numbers of 1.5, 2.0, and 3.1. The flight and wind-tunnel data for turbulent or transitional flow, with few exceptions, are near or within a data band of $\Delta(p_b/p) = 0.10$ about the curve, which is expressed by the following equation:

$$\frac{c}{k_1 h N_{Re}^{1/5}} = 0.55e^{20.5(p_b/p)}$$

The data above the data band are the $M = 3.10$ data of reference 2 for the higher $\frac{c}{hN_{Re}^{1/5}}$ values, the $M = 3.10$ data of reference 5 for $h/2 = 0.51$ centimeter (0.2 inch), and the $M = 3.5$ laminar flow data of reference 15. As previously stated, because of the Reynolds number range for a given Mach number, the data of reference 15 show that the base pressure ratio increases as the flow conditions change from near fully turbulent flow to fully laminar flow. When the base pressure data of reference 15 for $M = 3.5$ for the Reynolds number range of the study are plotted in figure 11, the data approaching fully laminar flow are above the data band. The laminar flow data for $M = 2.5$ and $M = 5.0$, which are not plotted, show the same trend. Thus, it appears that other data above the data band, which are also inconsistent with the criteria of reference 15 (see fig. 9(b)), may have more laminar than turbulent or transitional flow characteristics at the base in the supersonic Mach number range.

The method of presentation used in figure 11 may be useful in comparing turbulent or transitional flow base pressure data for both a rather wide range of momentum-thickness-to-base-width ratios (0.002 to 0.20) and a range of supersonic Mach numbers. In addition, the method seems to provide another criterion for determining whether the flow is laminar or whether transition occurs near or before separation. More study is needed to fully determine the real worth of the method.

Base pressure difference.— In reference 18, data were presented as a base pressure difference, $p_b - p$, versus p. For each specific Mach number and step height, the $p_b - p$ versus p curves were linear. The X-15 flight data also show a linear relationship for both $p_b - p$ versus p (fig. 12) and $p_b - p$ versus q (fig. 13) for Mach numbers from 1.5 to 5.0. The slopes of the faired lines in figures 12 and 13 are shown in figures 14(a) and 14(b), respectively. The wind-tunnel data of reference 18 for step heights of 1.13 centimeters (0.443 inch) and 1.91 centimeters (0.750 inch) are in good agreement with the flight data. Next, from the definition for base pressure coefficient,

$$C_{p,b} = \frac{p_b - p}{0.7M^2 p} = \frac{p_b - p}{q}$$

the slopes were calculated for the flight and wind-tunnel data. For a first approximation, the slopes were found by assuming the base pressure coefficient was constant for a

specific Mach number. Then the slopes would be

$$\frac{d(p_b - p)}{dp} = 0.7M^2C_{p,b} \tag{1}$$

and

$$\frac{d(p_b - p)}{dq} = C_{p,b} \tag{2}$$

However, as shown in figures 14(a) and 14(b), these calculated values for the present study and for reference 18 are consistently less negative than their respective experimental slopes. This suggests that dynamic pressure is not an adequate normalizing quantity for the base pressure coefficient, and, therefore, base pressure coefficient could vary because of variations in dynamic pressure (and, hence, free-stream static pressure) at a specific Mach number.

If the base pressure coefficient were not constant for a given Mach number, the slopes would become

$$\frac{d(p_b - p)}{dp} = 0.7M^2C_{p,b} + q\frac{dC_{p,b}}{dp}$$

and

$$\frac{d(p_b - p)}{dq} = C_{p,b} + q\frac{dC_{p,b}}{dq}$$

Because the data of the present study and of reference 18 do vary with q (and, hence, p), the difference between the calculated and experimental slopes would be in the $dC_{p,b}/dq$ and $dC_{p,b}/dp$ terms. The variation in p would also cause a corresponding variation in Reynolds number. The range in Reynolds number for the X-15 data is relatively small, and the data remain in the turbulent flow region; however, in reference 18 the Reynolds number range is from 2.33×10^5 to 1.67×10^6, and the data are in the near laminar to near turbulent flow regions, i.e., the transitional region.

From fairings of the flight data, the experimental slopes for $\frac{d(p_b - p)}{dp}$ (fig. 14(a)) can be approximated by the linear equations

$$\frac{d(p_b - p)}{dp} = -0.346M - 0.117 \text{ (for } M = 1.5 \text{ to } 2.4)$$

and

$$\frac{d(p_b - p)}{dp} = -0.02M - 0.90 \text{ (for } M = 2.4 \text{ to } 5.0)$$

Similarly, for the slopes of $\frac{d(p_b - p)}{dq}$ (fig. 14(b)), the curves

$$\frac{d(p_b - p)}{dq} = \frac{-0.407}{0.7M^2} - 0.138 \quad (\text{for } M = 1.5 \text{ to } 2.4)$$

and

$$\frac{d(p_b - p)}{dq} = \frac{-0.980}{0.7M^2} - 0.002 \quad (\text{for } M = 2.4 \text{ to } 5.0)$$

are good approximations. The slopes of the curves for the experimental values of both $\frac{d(p_b - p)}{dp}$ and $\frac{d(p_b - p)}{dq}$ change near $M = 2.4$. This change may be related to an increase in the lip shock[1] effects, because in reference 19 the effect of lip shock which is not noticeable either at $M = 1.5$ or 2.0 becomes apparent at $M = 2.4$ and is quite noticeable at $M = 3.0$.

CONCLUSIONS

Analysis of the power-off base pressures measured on the X-15 airplane for Mach numbers from 1.5 to 5.0 and comparison with theory, semiempirical estimates, and wind-tunnel results showed that:

1. By using a derived Mach-number-dependent factor, the base pressure ratio can be presented as a linearized function of turbulent boundary-layer height and base width for turbulent or transitional flow at the base. Therefore, the flight and wind-tunnel data can be compared for the range of Mach numbers between 1.5 and 5.0 instead of only at the most studied Mach numbers of 1.5, 2.0, and 3.1. In addition, this method seemed to provide another criterion for observing whether flow is laminar or turbulent.

2. At any specific Mach number of the study, the difference between base and free-stream pressure was a linear function of both free-stream pressure and dynamic pressure.

3. Speed-brake position influenced the pressure on adjacent base elements, which represented an example of communication between nearby base elements.

4. The difference between base pressures for the sharp-leading-edge fin of this study and the blunt-leading-edge fin of a previous study was negligible, indicating that the inviscid effects of a blunt leading edge appear to have no influence when the ratio of the chord length to the diameter of the leading edge of the vertical fin, c/d, is approximately 100 or larger.

---

[1]A shock wave emanating from the separation edge of the base.

5. The variation in pressure over the base of the sharp-leading-edge upper vertical fin, as measured at six locations, was negligible for a specific flight condition. Hence, for most practical purposes, the base pressure for this surface could be adequately defined from one location.

Flight Research Center,
National Aeronautics and Space Administration,
Edwards, Calif., December 4, 1970.

APPENDIX

DEVELOPMENT OF EQUATION FOR CALCULATING k_1

Define an equation

$$\frac{c}{hN_{Re}^{1/5}} = k_1 e^{B(p_b/p)} \tag{A1}$$

where B is a constant and k_1 is constant for any specific Mach number between 1.5 and 5.0. Because the base pressure ratios of Chapman et al. (ref. 2) show an essentially linear variation with $\frac{c}{hN_{Re}^{1/5}}$ for Mach numbers of 1.5, 2.0, and 3.1, the slopes of these lines can be used to calculate B.

The quantity k_1 is a constant for a specific Mach number, so B for a given Mach number is found by choosing two points on the M = constant curve. Then, from equation (A1),

$$\frac{\left(\frac{c}{hN_{Re}^{1/5}}\right)_2}{\left(\frac{c}{hN_{Re}^{1/5}}\right)_1} = \frac{k_1 e^{B(p_b/p)_2}}{k_1 e^{B(p_b/p)_1}} = e^{B[(p_b/p)_2 - (p_b/p)_1]}$$

so

$$B = \frac{\log\left[\frac{\left(\frac{c}{hN_{Re}^{1/5}}\right)_2}{\left(\frac{c}{hN_{Re}^{1/5}}\right)_1}\right]}{((p_b/p)_2 - (p_b/p)_1)\log e}$$

where log is a common logarithm, or

$$B = 2.3026\frac{\log\left(\frac{c}{hN_{Re}^{1/5}}\right)_2 - \log\left(\frac{c}{hN_{Re}^{1/5}}\right)_1}{(p_b/p)_2 - (p_b/p)_1} \tag{A2}$$

Values of B calculated from equation (A2) for each of the Mach numbers of reference 2 were $B_{1.5} = 31.4$, $B_{2.0} = 21.4$, and $B_{3.1} = 8.8$. These three values were then averaged, and the average value of 20.5 was used for Mach numbers from 1.5 to 5.0. Therefore, equation (A1) becomes

APPENDIX

$$k_1 = \left(\frac{c}{hN_{Re}^{1/5}}\right)\left(1/e^{20.5p_b/p}\right) \tag{A3}$$

Average values of k_1 were calculated from equation (A3) for Mach numbers of 1.5, 2.0, and 3.1 using the wind-tunnel data of reference 2 and the flight data of reference 7 (wing data only) and an average of the data for speed brakes closed and opened of the present study. Other values of k_1 between Mach numbers from 1.5 to 5.0 were calculated from an average of the speed-brakes-closed and speed-brakes-opened data. The variation of k_1 with Mach number is shown in figure 15.

REFERENCES

1. Korst, H. H.: A Theory for Base Pressures in Transonic and Supersonic Flow. J. Appl. Mech., vol. 23, no. 4, Dec. 1956, pp. 593-600.

2. Chapman, Dean R.; Wimbrow, William R.; and Kester, Robert H.: Experimental Investigation of Base Pressure on Blunt-Trailing-Edge Wings at Supersonic Velocities. NACA Rep. 1109, 1952. (Supersedes NASA TN 2611.)

3. Nash, J. F.: An Analysis of Two-Dimensional Turbulent Base Flow, Including the Effect of the Approaching Boundary Layer. NPL Aero Rep. 1036, British A.R.C., July 30, 1962.

4. Nash, J. F.: A Discussion of Two-Dimensional Turbulent Base Flows. NPL Aero Rep. 1162, British A.R.C., July 20, 1965.

5. Hastings, R. C.: Turbulent Flow Past Two-Dimensional Bases in Supersonic Streams. British R. & M. No. 3401, 1965.

6. Saltzman, Edwin J.: Preliminary Base Pressures Obtained From the X-15 Airplane at Mach Numbers From 1.1 to 3.2. NASA TN D-1056, 1961.

7. Saltzman, Edwin J.: Base Pressure Coefficients Obtained From the X-15 Airplane for Mach Numbers up to 6. NASA TN D-2420, 1964.

8. Mechtly, E. A.: The International System of Units - Physical Constants and Conversion Factors. NASA SP-7012, 1969.

9. Webb, Lannie D.: Characteristics and Use of X-15 Air-Data Sensors. NASA TN D-4597, 1968.

10. Beers, Yardley: Introduction to the Theory of Error. Second ed., Addison-Wesley Publishing Co., 1962.

11. Garringer, Darwin J.; and Saltzman, Edwin J.: Flight Demonstration of a Skin-Friction Gage to a Local Mach Number of 4.9. NASA TN D-3830, 1967.

12. McLain, L. J.; and Palitz, Murray: Flow-Field Investigations on the X-15 Airplane and Model Up to Hypersonic Speeds. NASA TN D-4813, 1968.

13. Hama, Francis R.: Experimental Investigations of Wedge Base Pressure and Lip Shock. JPL Tech. Rep. 32-1033, Jet Prop. Lab., Dec. 1, 1966.

14. Larson, R. E.; Scott, C. J.; Elgin, D. R.; and Seiver, R. E.: Turbulent Base Flow Investigations at Mach Number 3. Univ. of Minnesota (NASA CR-55718), 1962.

15. Smith, Howard E.: The Flow Field and Heat Transfer Downstream of a Rearward Facing Step in Supersonic Flow. ARL 67-0056, Aero. Res. Lab., U.S. Air Force, March 1967. (Available from ASTIA as AD 655 370.)

16. Saltzman, Edwin J. ; and Garringer, Darwin J. : Summary of Full-Scale Lift and Drag Characteristics of the X-15 Airplane. NASA TN D-3343, 1966.

17. Chapman, Dean R. : An Analysis of Base Pressure at Supersonic Velocities and Comparison With Experiment. NACA Rep. 1051, 1951. (Supersedes NACA TN 2137.)

18. Scherberg, Max G. ; and Smith, Howard E. : An Experimental Study of Supersonic Flow over a Rearward Facing Step. AIAA J., vol. 5, no. 1, Jan. 1967, pp. 51-56.

19. Kessler, Thomas J. : A Theory for Two-Dimensional Supersonic Turbulent Base Flows. AIAA Paper 69-68, Jan., 1969.

TABLE 1. PHYSICAL CHARACTERISTICS OF THE X-15 AIRPLANE

Wing —	
Airfoil section	NACA 66005 (modified)
Total area (includes 8.82 m^2 (94.98 ft^2) covered by fuselage), m^2 (ft^2)	18.58 (200)
Span, m (ft)	6.82 (22.36)
Mean aerodynamic chord, m (ft)	3.13 (10.27)
Root chord, m (ft)	4.54 (14.91)
Tip chord, m (ft)	0.91 (2.98)
Taper ratio	0.20
Aspect ratio	2.50
Sweep at leading edge, deg	36.75
Sweep at 25-percent-chord line, deg	25.64
Sweep at trailing edge, deg	-17.74
Incidence, deg	0
Horizontal tail —	
Airfoil section	NACA 66005 (modified)
Total area (includes 5.88 m^2 (63.29 ft^2) covered by fuselage), m^2 (ft^2)	10.72 (115.34)
Span, m (ft)	5.51 (18.08)
Mean aerodynamic chord, m (ft)	2.15 (7.05)
Root chord, m (ft)	3.12 (10.22)
Tip chord, m (ft)	0.64 (2.11)
Taper ratio	0.21
Aspect ratio	2.83
Sweep at leading edge, deg	50.58
Sweep at 25-percent-chord line, deg	45
Sweep at trailing edge, deg	19.28
Ratio horizontal-tail area to wing area	0.58
Lower vertical tail —	
Airfoil section	10° single wedge
Area (excluding area covered by fuselage), m^2 (ft^2)	3.20 (34.41)
Span, m (ft)	1.88 (6.17)
Mean aerodynamic chord, m (ft)	2.80 (9.17)
Root chord, m (ft)	3.11 (10.21)
Tip chord, m (ft)	2.44 (8.00)
Taper ratio	0.78
Aspect ratio	0.43
Sweep at leading edge, deg	30
Sweep at 25-percent-chord line, deg	23.41
Ratio vertical-tail area to wing area	0.17
Speed-brake total surface area, m^2 (ft^2)	1.04 (11.18)
Fuselage —	
Length, m (ft)	15.09 (49.5)
Maximum width, m (ft)	2.23 (7.33)
Maximum depth, m (ft)	1.42 (4.67)
Maximum depth over canopy, m (ft)	1.51 (4.97)
Side area (total), m^2 (ft^2)	20.03 (215.66)
Fineness ratio	10.91
Sweep at canopy leading edge, deg	60

TABLE 2. PHYSICAL CHARACTERISTICS OF THE UPPER VERTICAL FIN OF THE X-15 AIRPLANE

	Blunt leading edge (ref. 7)	Sharp leading edge
Airfoil section	10° single wedge	10° single wedge
Area (excluding area covered by fuselage), m^2 (ft^2)	3.80 (40.91)	3.93 (42.27)
Span, m (ft)	1.40 (4.58)	1.40 (4.58)
Root chord, m (ft)	3.11 (10.21)	3.11 (10.21)
Tip chord, m (ft)	2.30 (7.56)	2.44 (8.02)
Aspect ratio	0.51	0.50
Ratio vertical-tail area to wing area	0.20	0.21
Speed-brake-surface area, each, m^2 (ft^2)	0.50 (5.37)	0.50 (5.37)
Leading-edge diameter, cm (in.)	2.54 (1)	0.076 (0.03)

Blunt leading edge

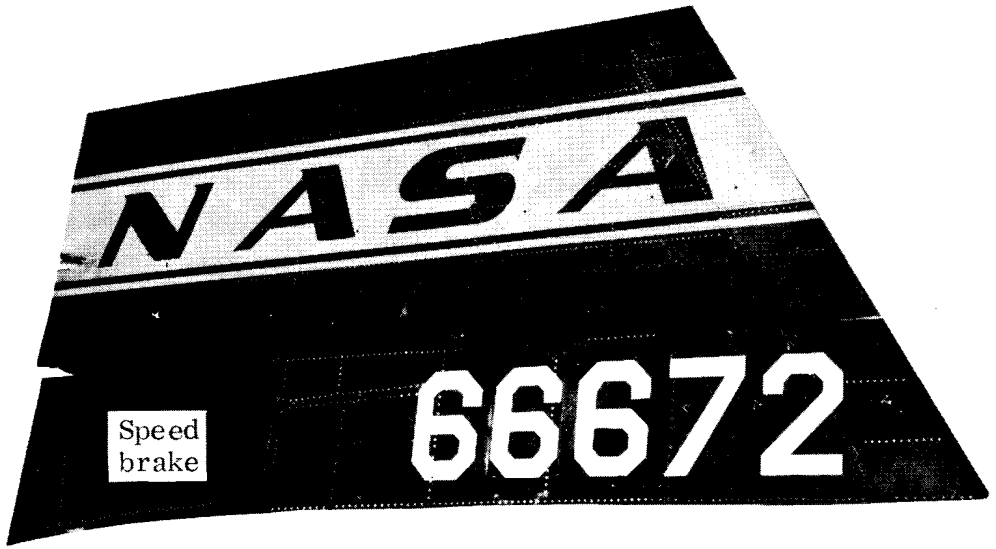

Sharp leading edge

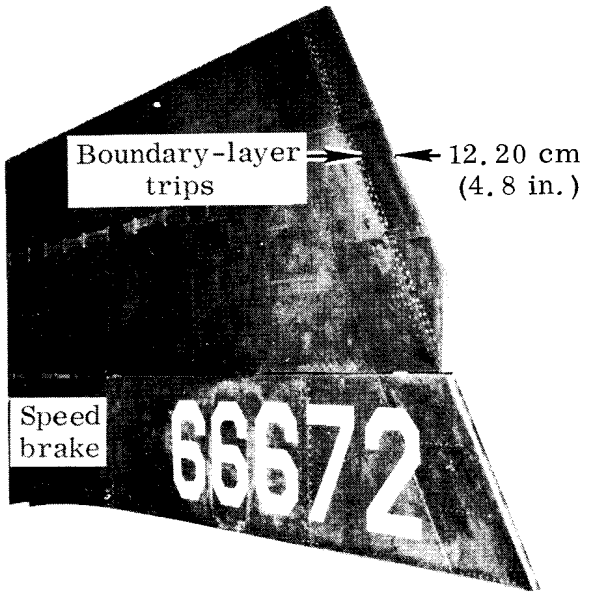

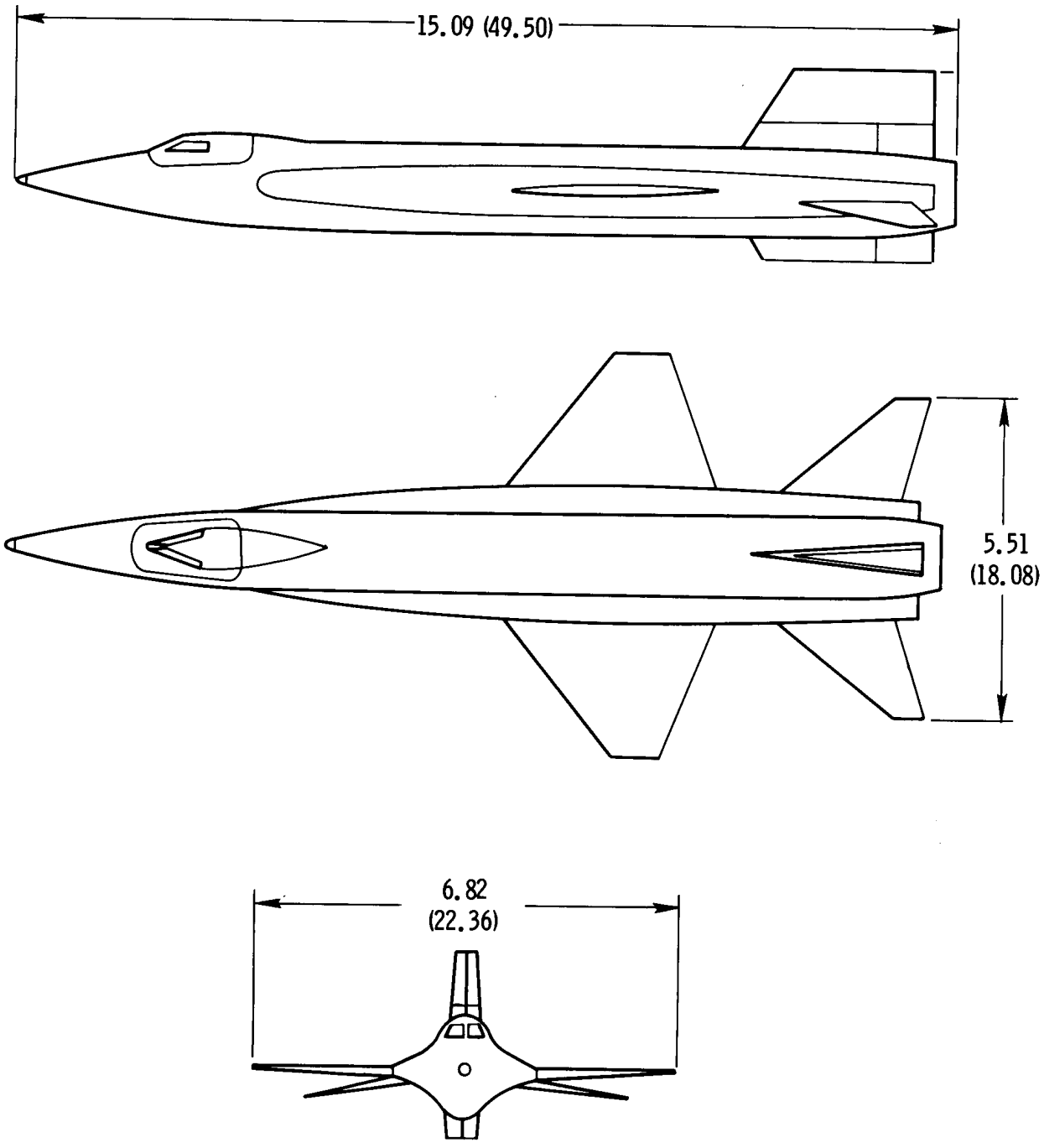

Figure 1. Three-view drawing of the X-15 airplane with the sharp-leading-edge vertical fin. Dimensions in meters (feet).

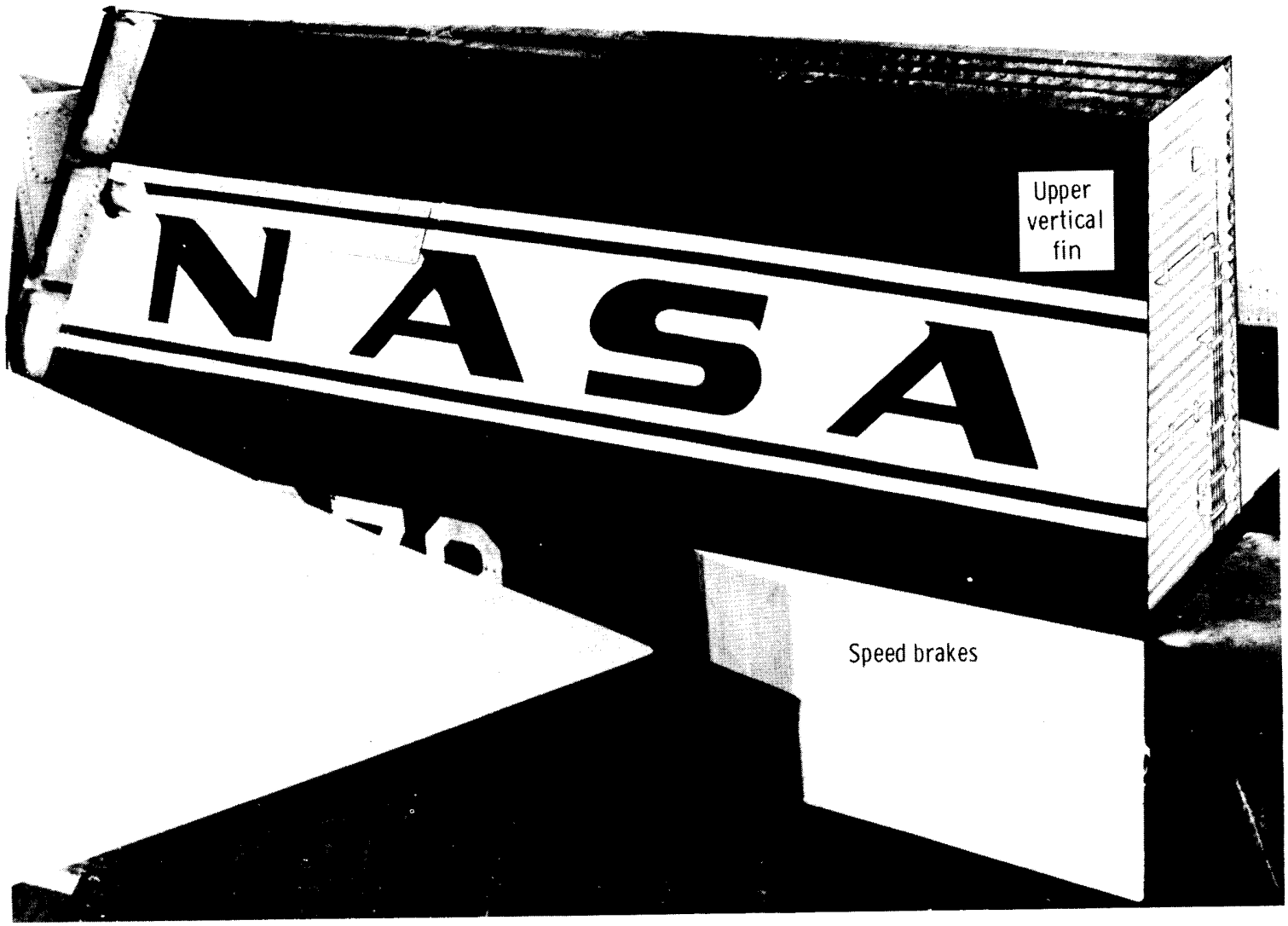

E-17600

Figure 2. Side view of the sharp-leading-edge upper vertical fin with the X-15 airplane mated to the B-52 airplane.

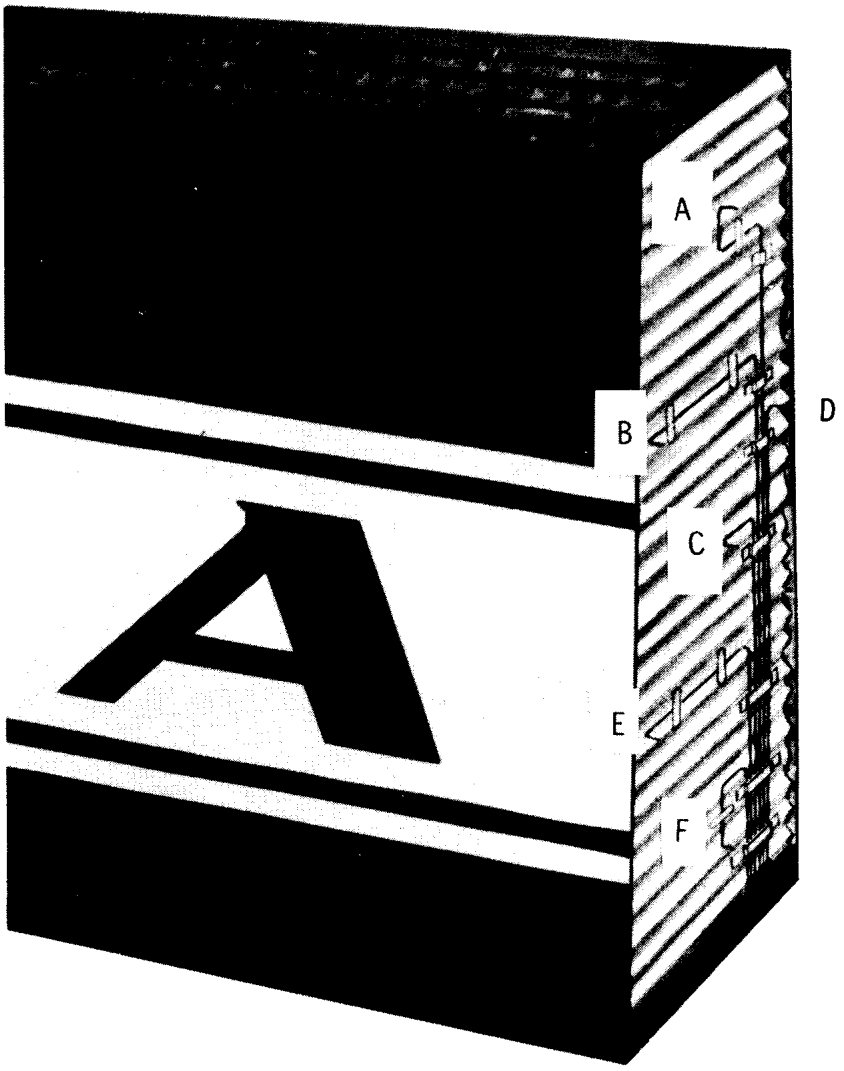

(a) Closeup of base region.

Figure 3. Photograph and sketch showing locations of the pressure taps on the base of the sharp-leading-edge fin.

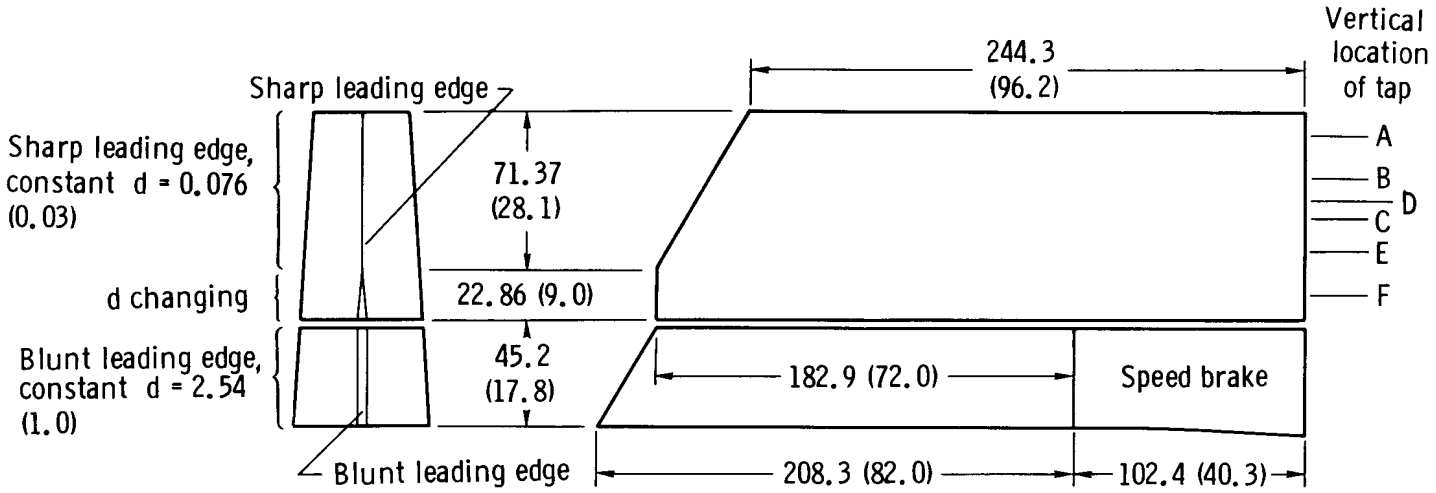

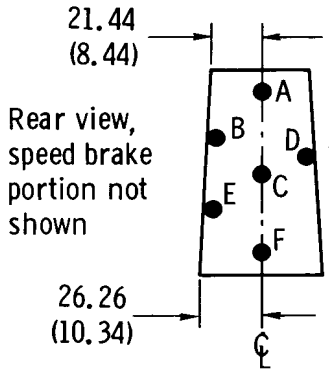

Tap	Distance from —		Distance from closest side
	Top	Bottom	
A	10.59 (4.17)	---	$\mathcal{L}$
B	30.48 (12)	---	2.69 (1.06)
C	---	45.72 (18)	$\mathcal{L}$
D	40.34 (15.88)	---	2.54 (1.00) [a]1.27 (0.50)
E	---	30.48 (12)	1.91 (0.75) [a]1.42 (0.56)
F	---	10.16 (4)	$\mathcal{L}$

[a]Distance after taps were moved closer to the edge of the fin.

(b) Sketch showing changes in the fin-leading-edge diameter and the location of the pressure taps (not drawn to scale). Dimensions in centimeters (inches).

Figure 3. Concluded.

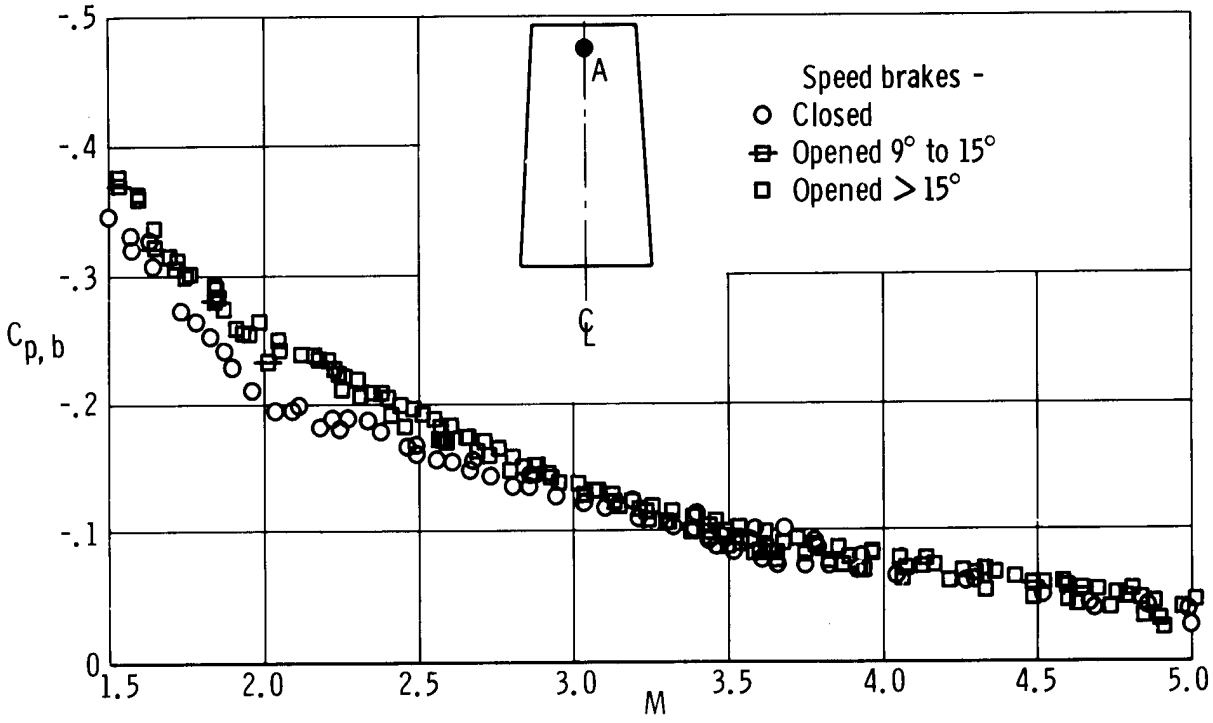

(a) Location A.

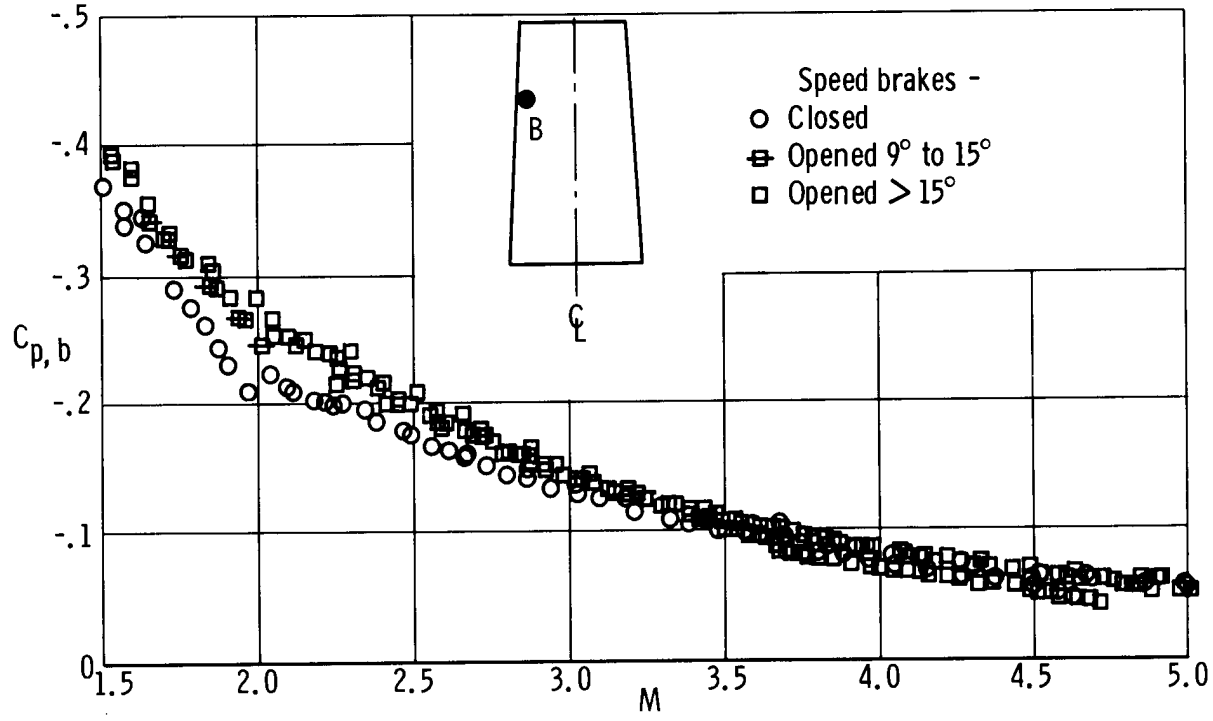

(b) Location B.

Figure 4. Base pressure coefficients from eight flights for each tap location on the sharp-leading-edge fin.

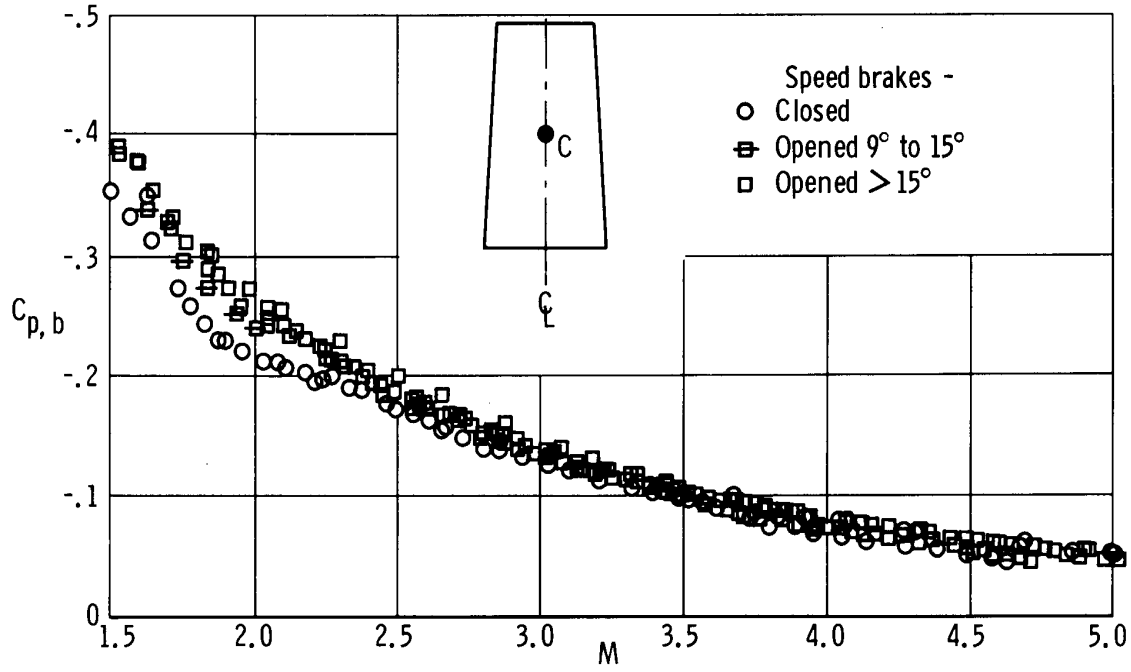

(c) Location C.

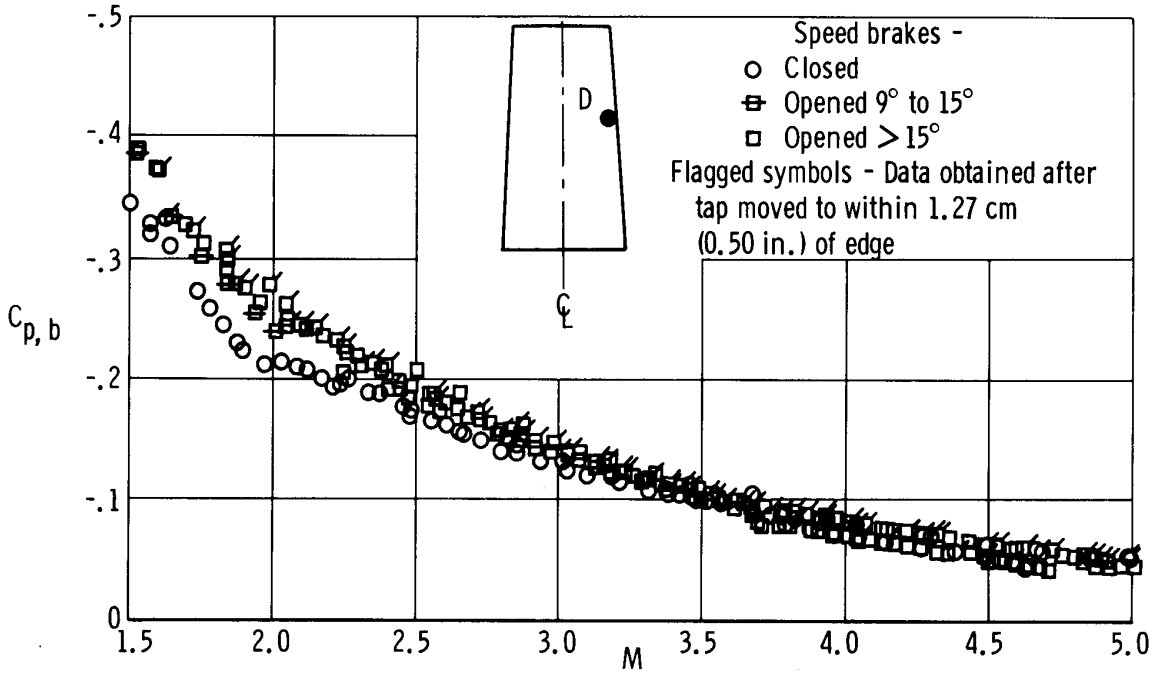

(d) Location D.

Figure 4. Continued.

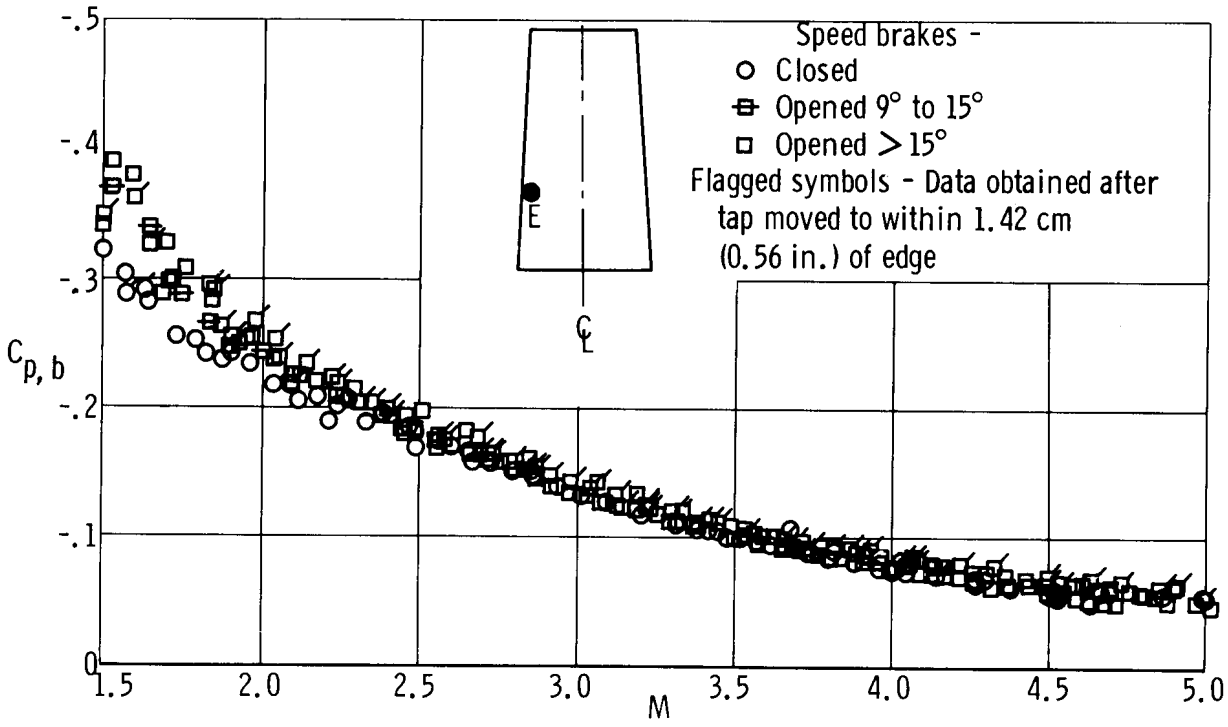

(e) Location E.

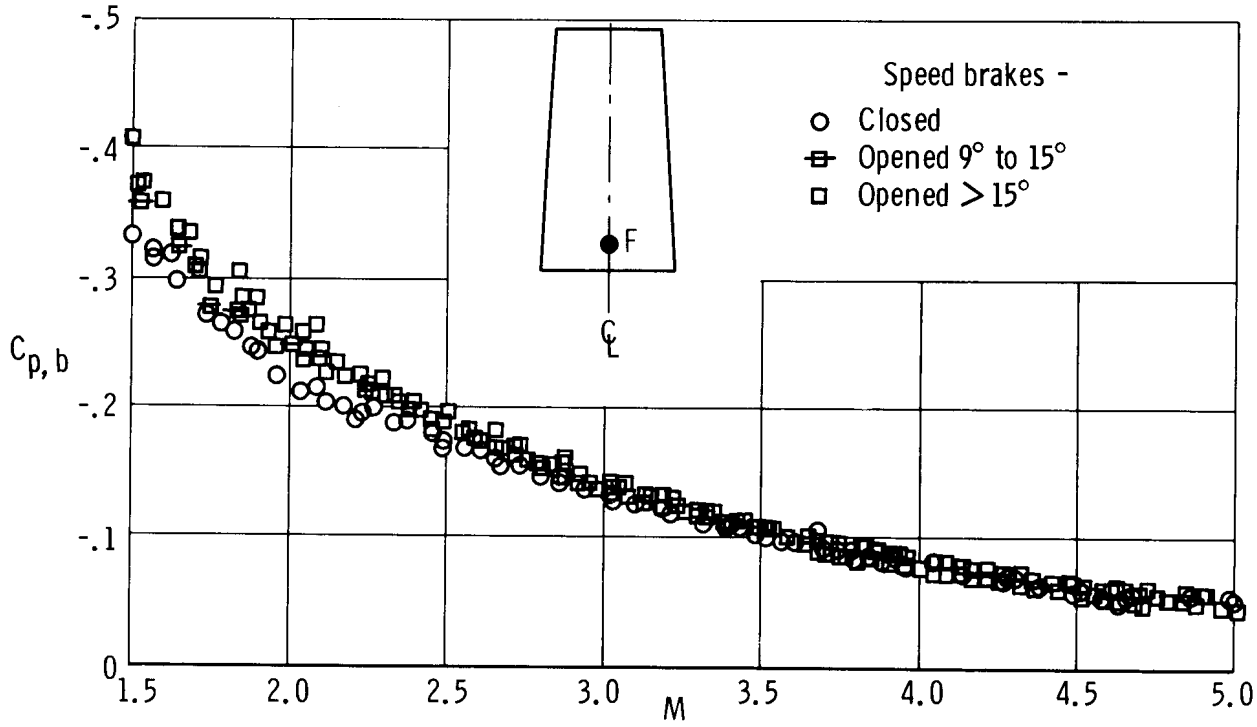

(f) Location F.

Figure 4. Concluded.

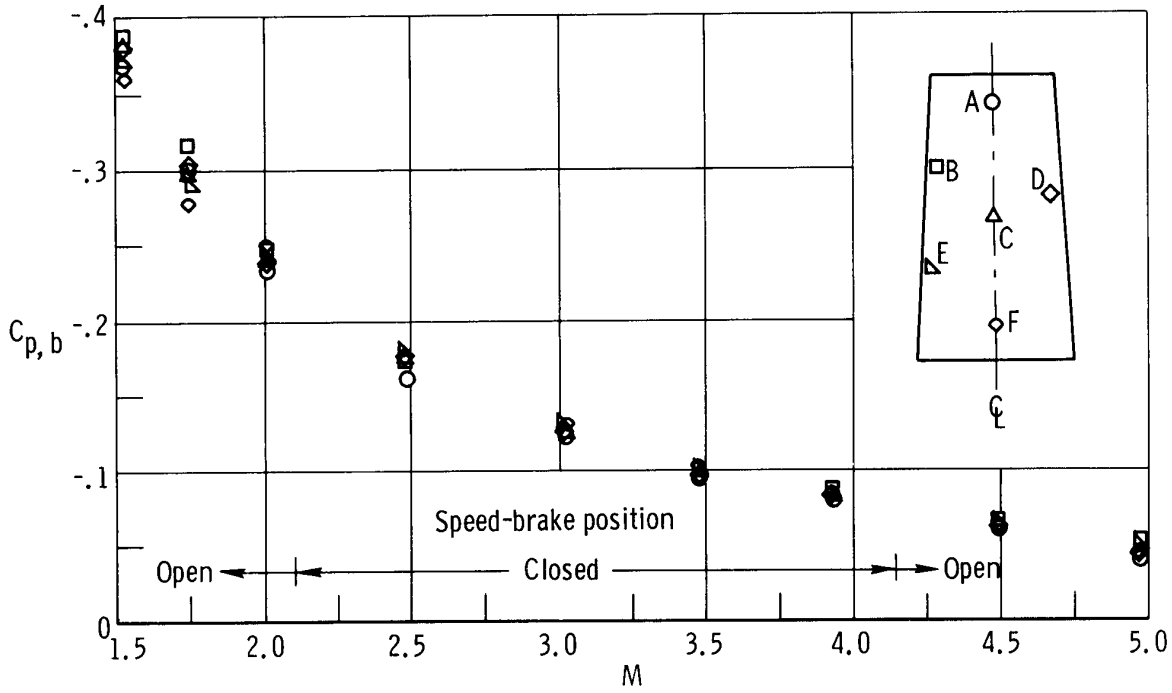

(a) Flight 1.

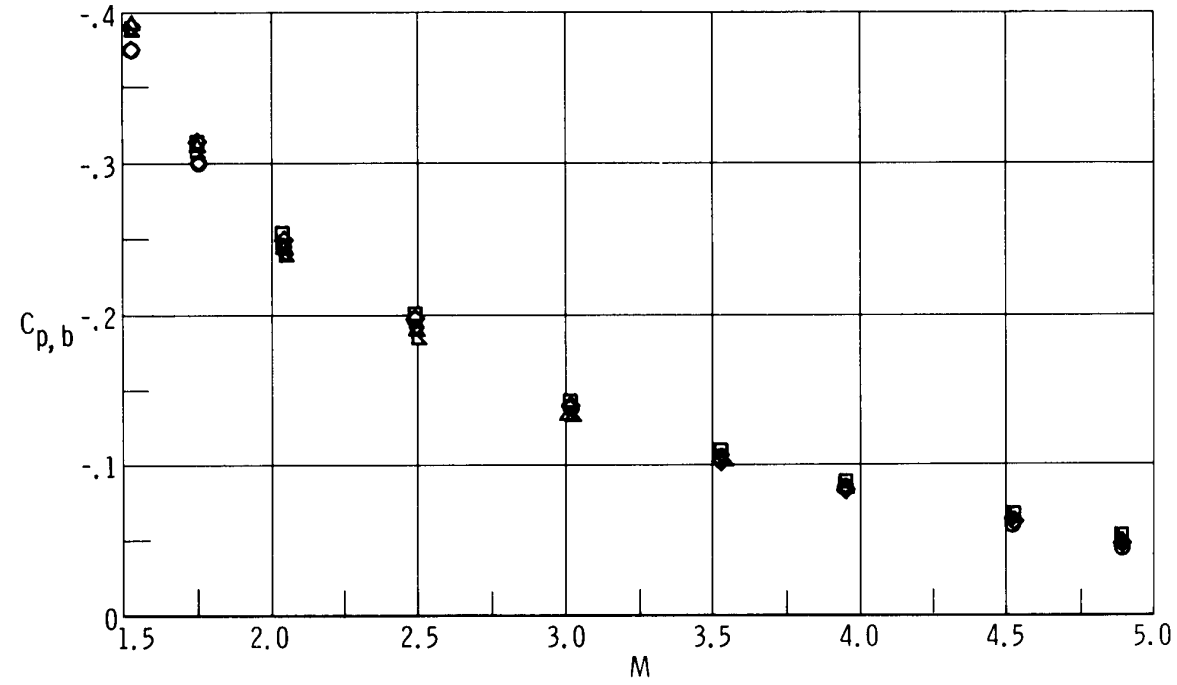

(b) Flight 2, speed brakes open.

Figure 5. Comparison of base pressure coefficients for all tap locations obtained on two typical flights on the sharp-leading-edge fin.

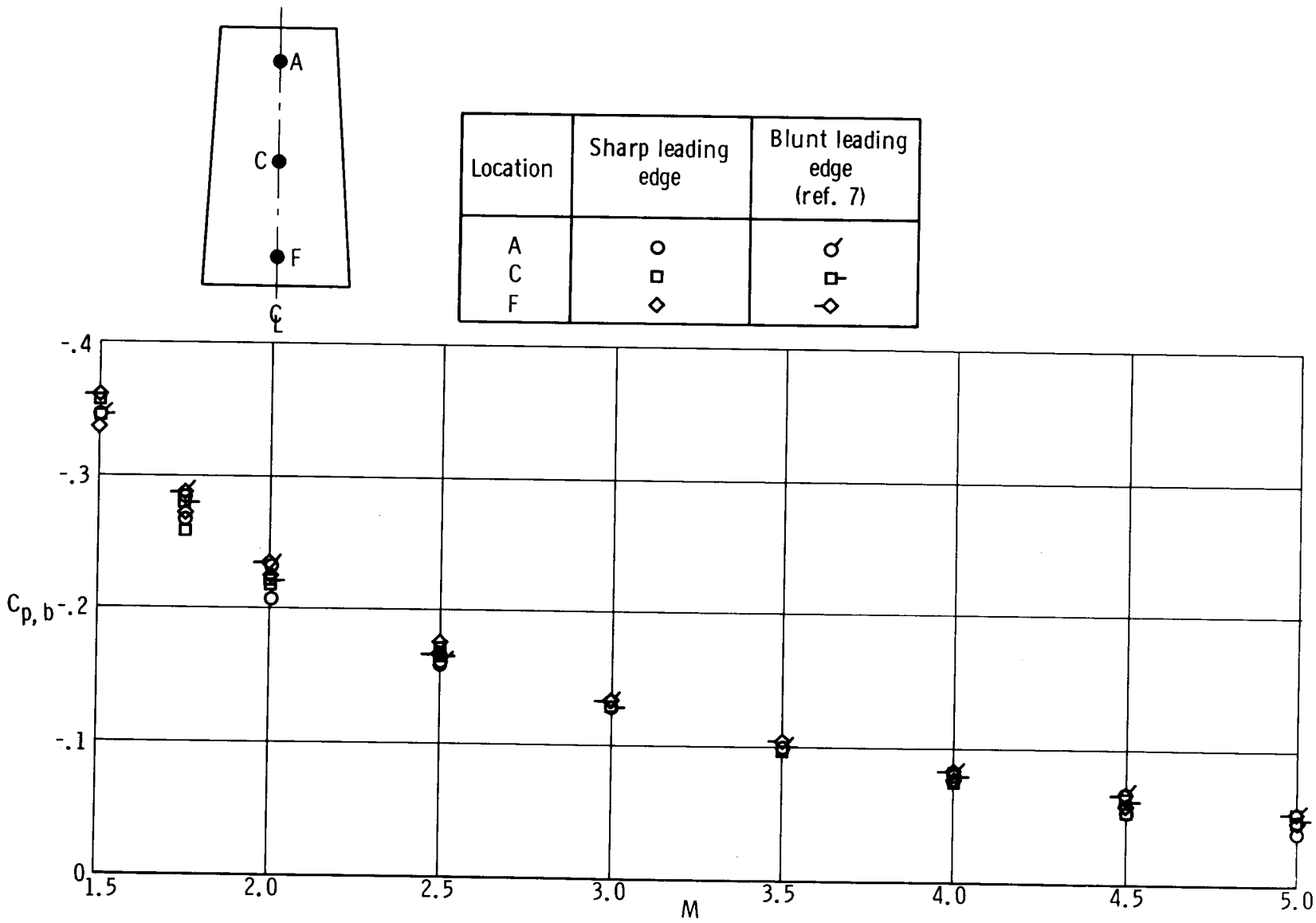

Figure 6. Comparison of average centerline base pressure coefficients for the sharp-leading-edge and blunt-leading-edge upper vertical fins. Speed brakes closed.

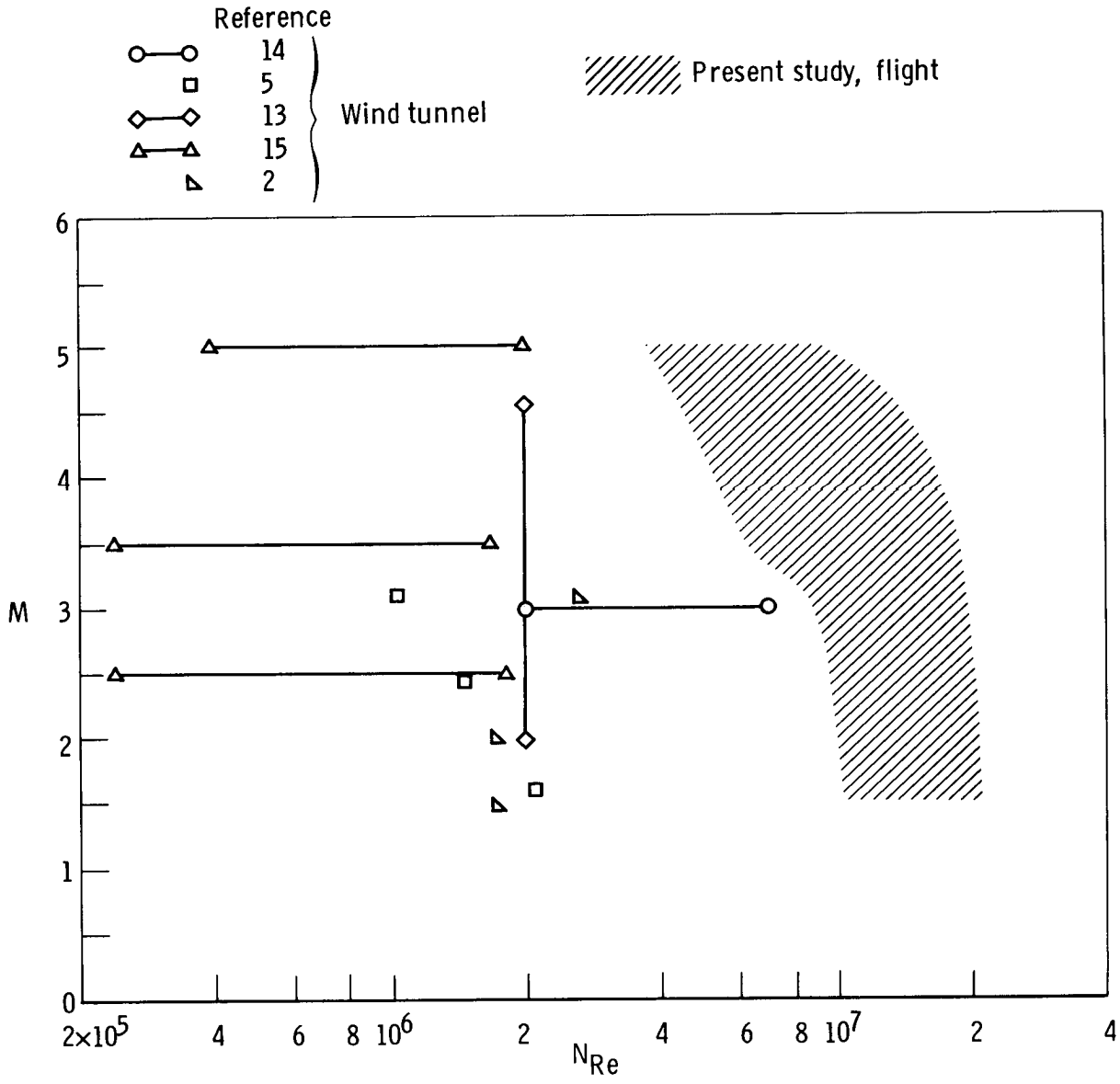

Figure 7. Comparison of flight Mach number and Reynolds number with wind-tunnel values.

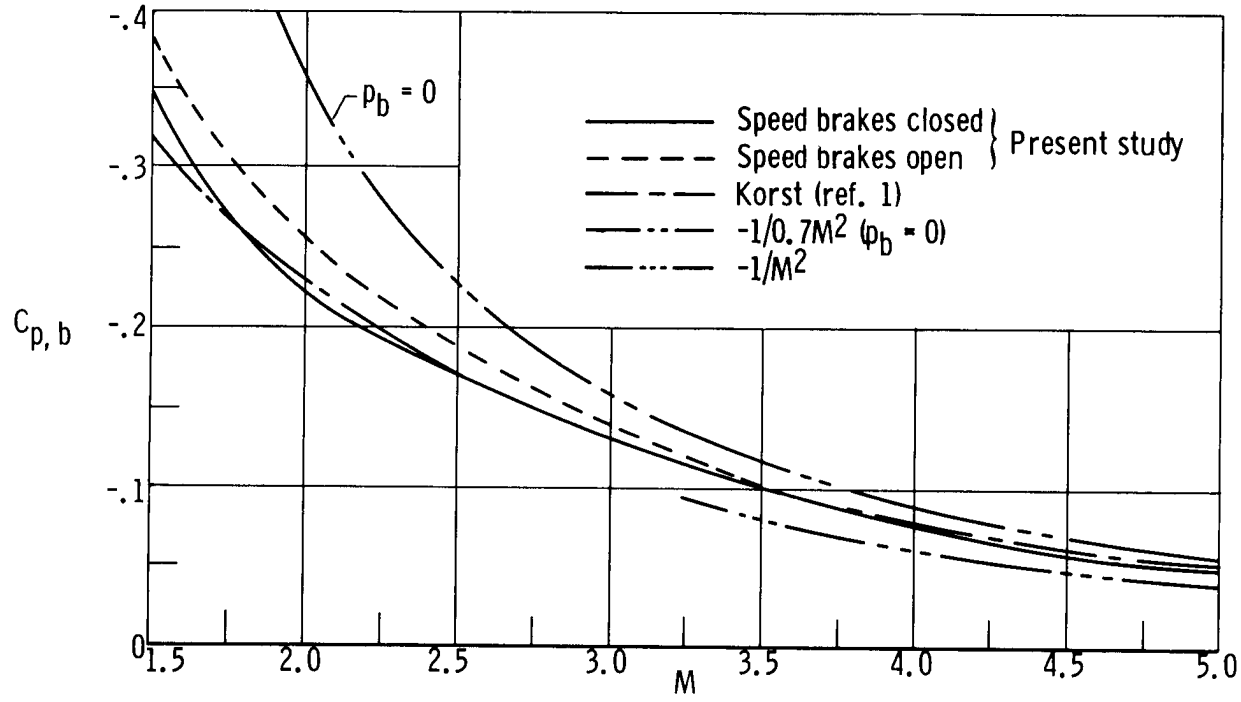

(a) Theoretical results.

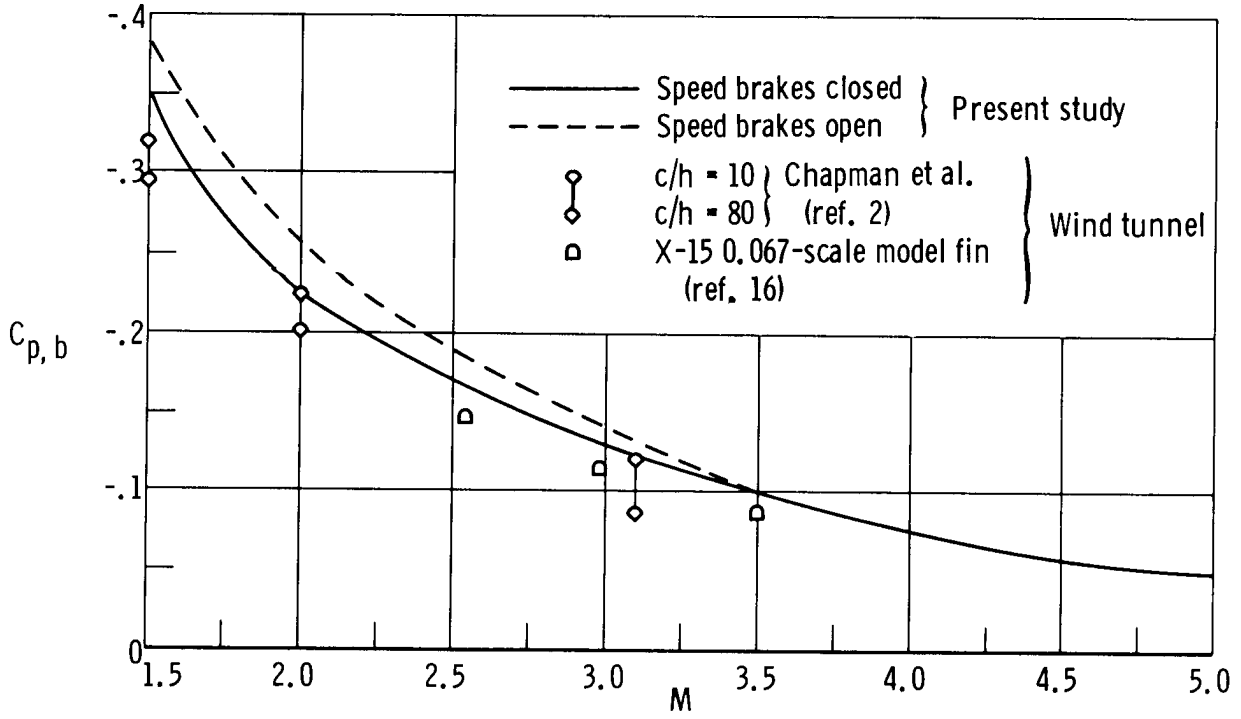

(b) Early wind-tunnel results.

Figure 8. Comparison of average flight base pressure coefficients with theoretical and wind-tunnel results.

	h, cm (in.)	c/h	N_{Re}	Reference
Speed brakes — Closed ——— Opened - - - -	47.70 (18.78)	5.6	3.83 to 21.10 × 10^6	Present study, wedge
○ ♂	[a]2.03 (0.8) [a]0.51 (0.2)	3.47 13.88	1.02 to 2.08 × 10^6	5, step
□	2.54 (1.0)	4.76	2.0 × 10^6	13, wedge
◇	3.81 (1.5)	5.5	7.0 × 10^6	14, wedge
△ ⏃	[a]1.91 (0.75) [a]1.13 (0.443)	2.67 4.52	1.68 to 2.00 × 10^6	15, step

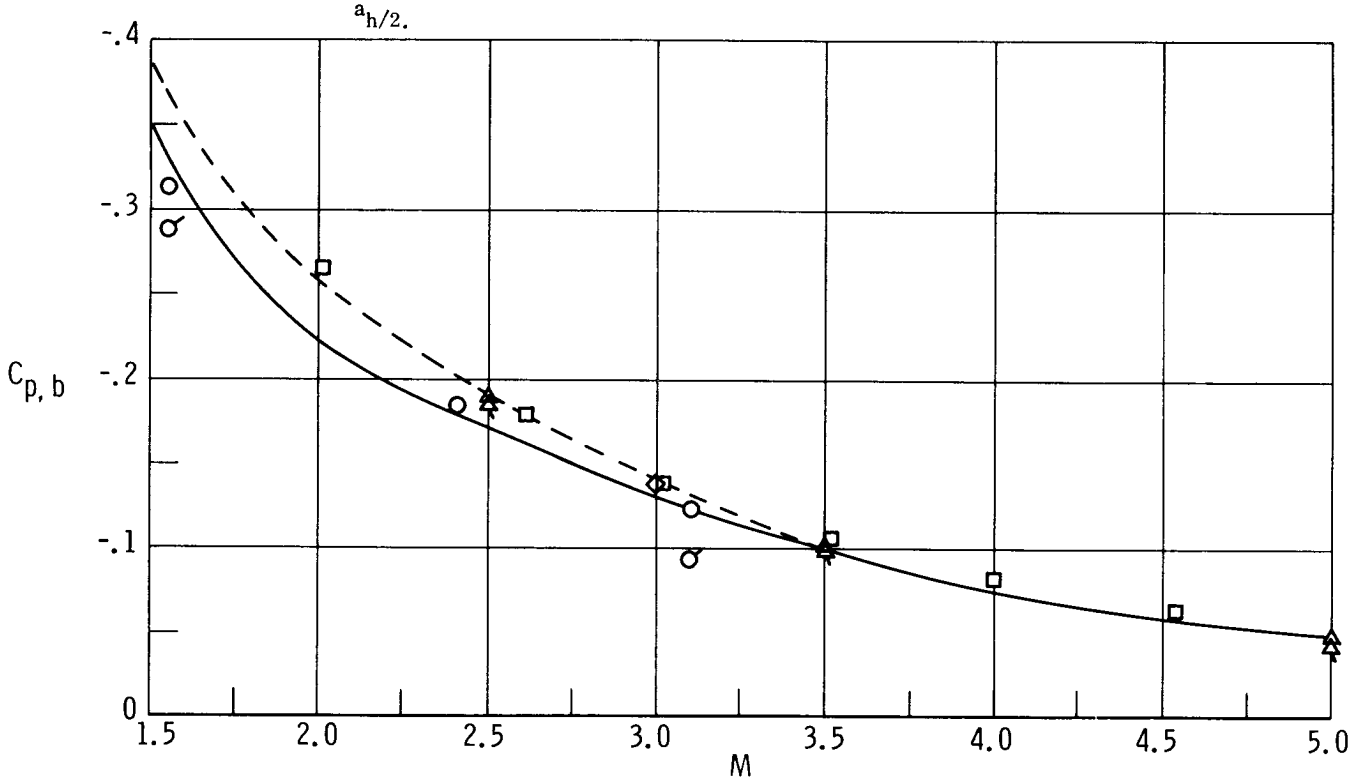

(c) Recent wind-tunnel results on wedges and steps.

Figure 8. Concluded.

	M	h, cm (in.)	Reference
Speed brakes — ○ □ Closed ◌ ◻ Opened	2.5, 3.5, 4.5, 3.0, 5.0	47.70 (18.78)	Present study
◇ ◇	3.10 2.41, 3.10	[a]0.51 (0.2) [a]2.03 (0.8)	5
△ ▽	2.61, 3.51, 4.54, 3.02	2.54 (1.0)	13
I	3.10	Varies	2
———	2.5, 3.5, 5.0	[a]1.91 (0.75)	15
— · —	3.0	3.81 (1.5)	14

[a]h 2.

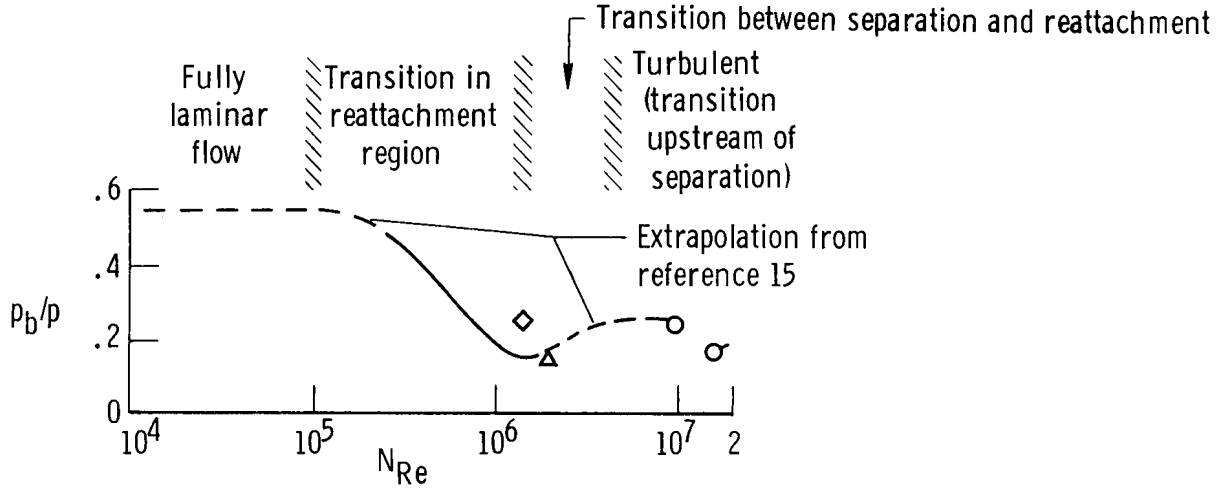

(a) M ≈ 2.5 (flow regions for M = 2.5 from reference 15).

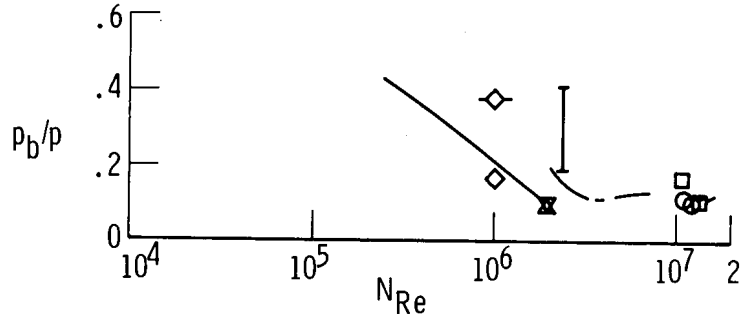

(b) M = 3.00 to 3.51.

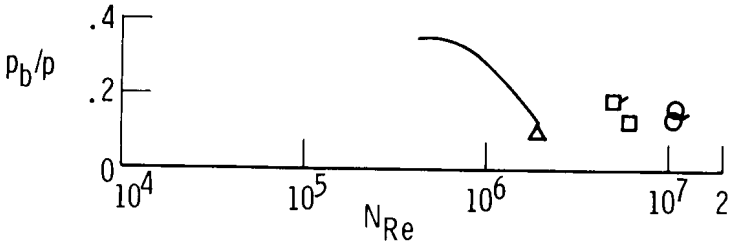

(c) M = 4.50 to 5.00.

Figure 9. Comparison of average flight base pressure ratio with wind-tunnel data as a function of Reynolds number.

	M	h, cm (in.)	N_{Re}	c/h	Source	Reference
○ □ ◇	1.50, 2.00, 3.00	47.70 (18.78)	10.5 to 13.9 × 10^6	5.6	X-15, flight	Present study
⊕ ⊞ ◈ ⊖ ⊟ ◈	1.50, 2.00, 3.10	47.12 (18.55) 2.69 (1.06)	6.0 to 22.1 × 10^6 6.4 to 23.6	5.5 103	X-15, flight	7
◻ ◇	2.01, 3.02	2.54 (1)	2 × 10^6	4.76	Wind tunnel	13
◇	3.00	3.81 (1.5)	2.7 × 10^6	5.5	Wind tunnel	14
◎ ◇ ⊖ ◈	1.56, 3.10	[a]2.03 (0.8) [a]0.51 (0.2)	1.02 to 2.08 × 10^6	3.47 13.88	Wind tunnel	5
——	1.50, 2.00, 3.10	0.10 to 0.87 (0.04 to 0.341)	1.7 to 2.6 × 10^6	10 to 80	Wind tunnel	2
● ■ ◆	1.50, 2.00, 3.10	Korst's thin-boundary-layer theory			Theory	1

[a] h/2.

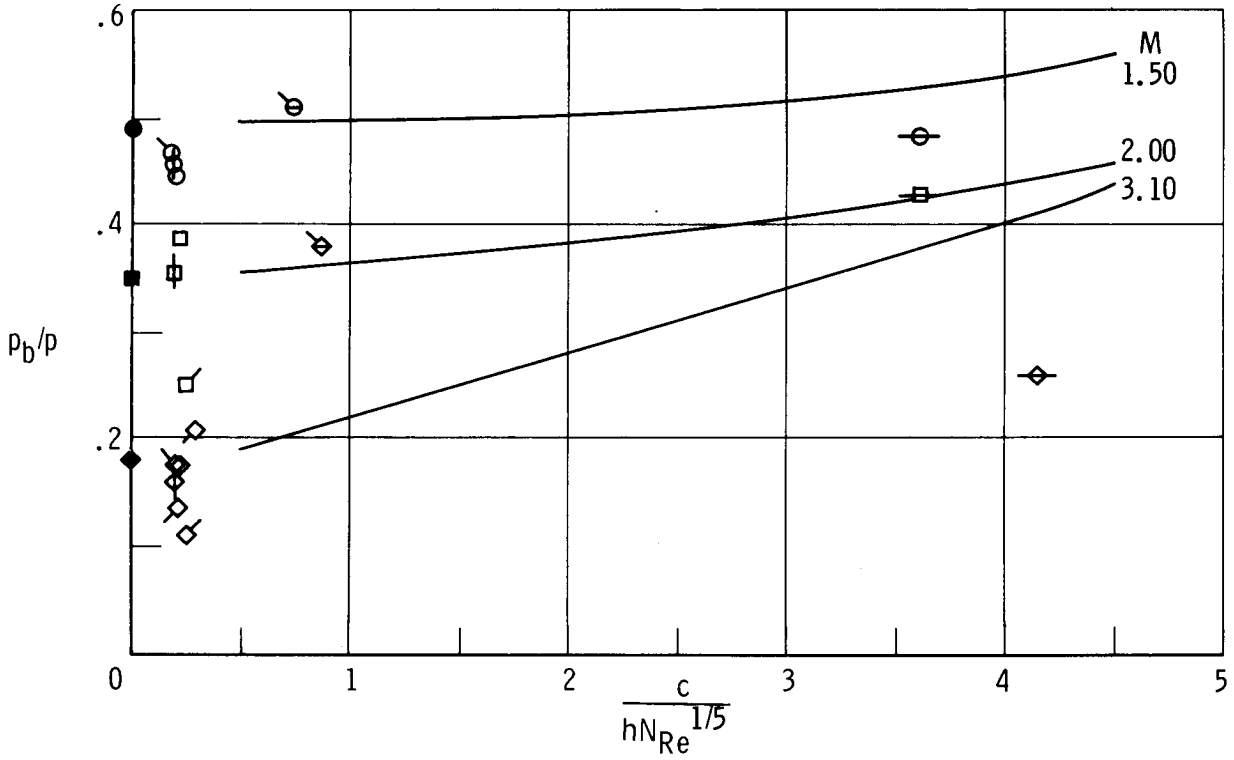

Figure 10. Comparison of average flight base pressure ratio with wind-tunnel data as a function of $\frac{c}{hN_{Re}^{1/5}}$. $M \approx 1.5$, 2.0, and 3.1; speed brakes closed.

	Reference	M	O/h
– – –	2	1.5 to 3.1	0.01 to 0.15
○ ⊖	Speed brakes closed } Present study Speed brakes opened }	1.5 to 5.0	0.006
□ ⊟	Fin } 7 Wing }	1.5 to 3.1	0.005 0.10
◇ ⊖	h/2 = 2.03 cm (0.8 in.) } 5 h/2 = 0.51 cm (0.2 in.) }	1.56 to 3.1	0.01 to 0.05
△	13	2.01 to 4.54	0.006
◺	14	3.00	0.005
◺ ⊟	h/2 = 1.91 cm (0.75 in.) } 15 h/2 = 1.13 cm (0.443 in.) }	2.5 to 5.0	0.002 to 0.02
◇	4	1.5 to 2.0	0.01 to 0.2

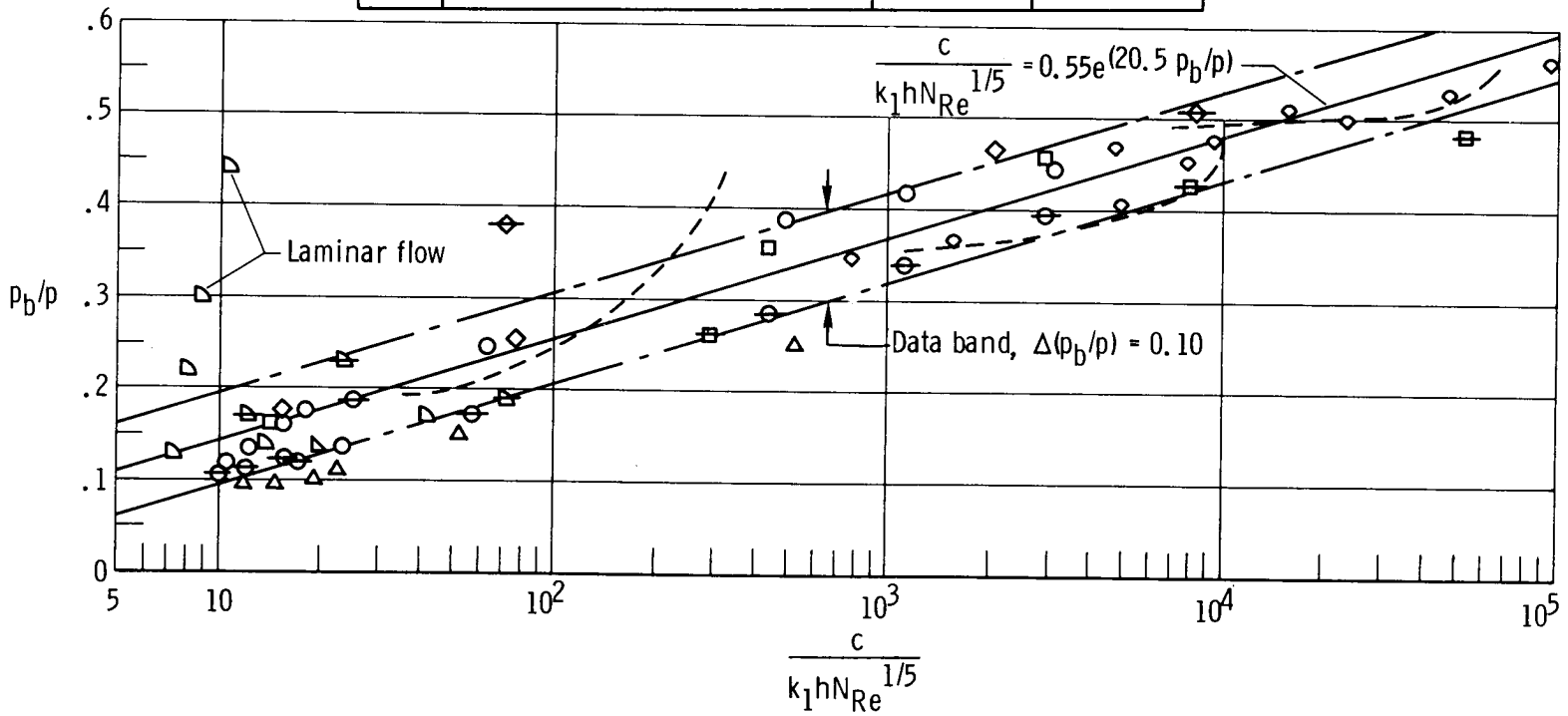

Figure 11. Comparison of average flight base pressure ratio with wind-tunnel and semiempirical data as a function of $\frac{c}{k_1 h N_{Re}^{1/5}}$. M = 1.5 to 5.0.

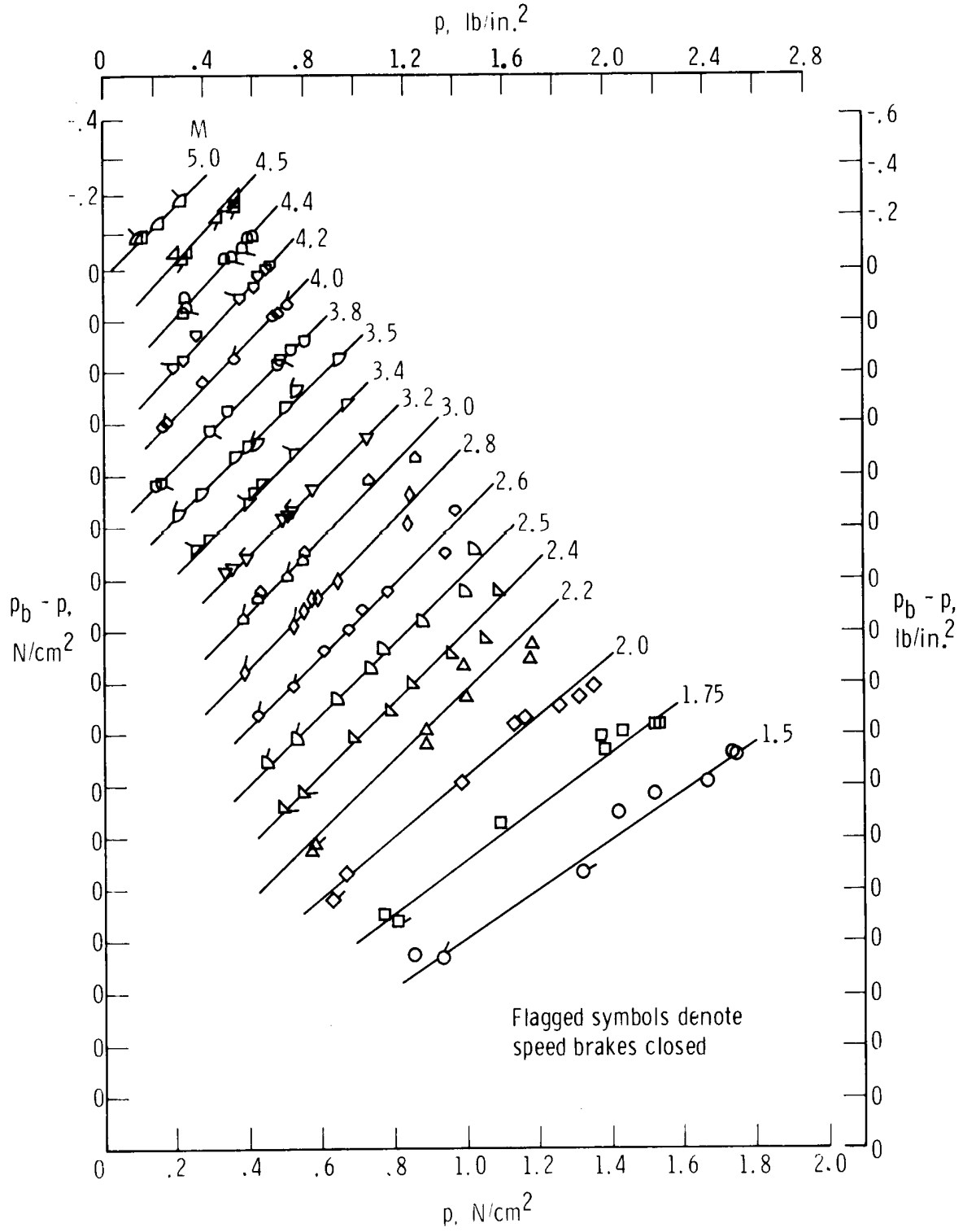

Figure 12. Difference between base pressure and free-stream pressure as a function of free-stream pressure for the X-15 flight data.

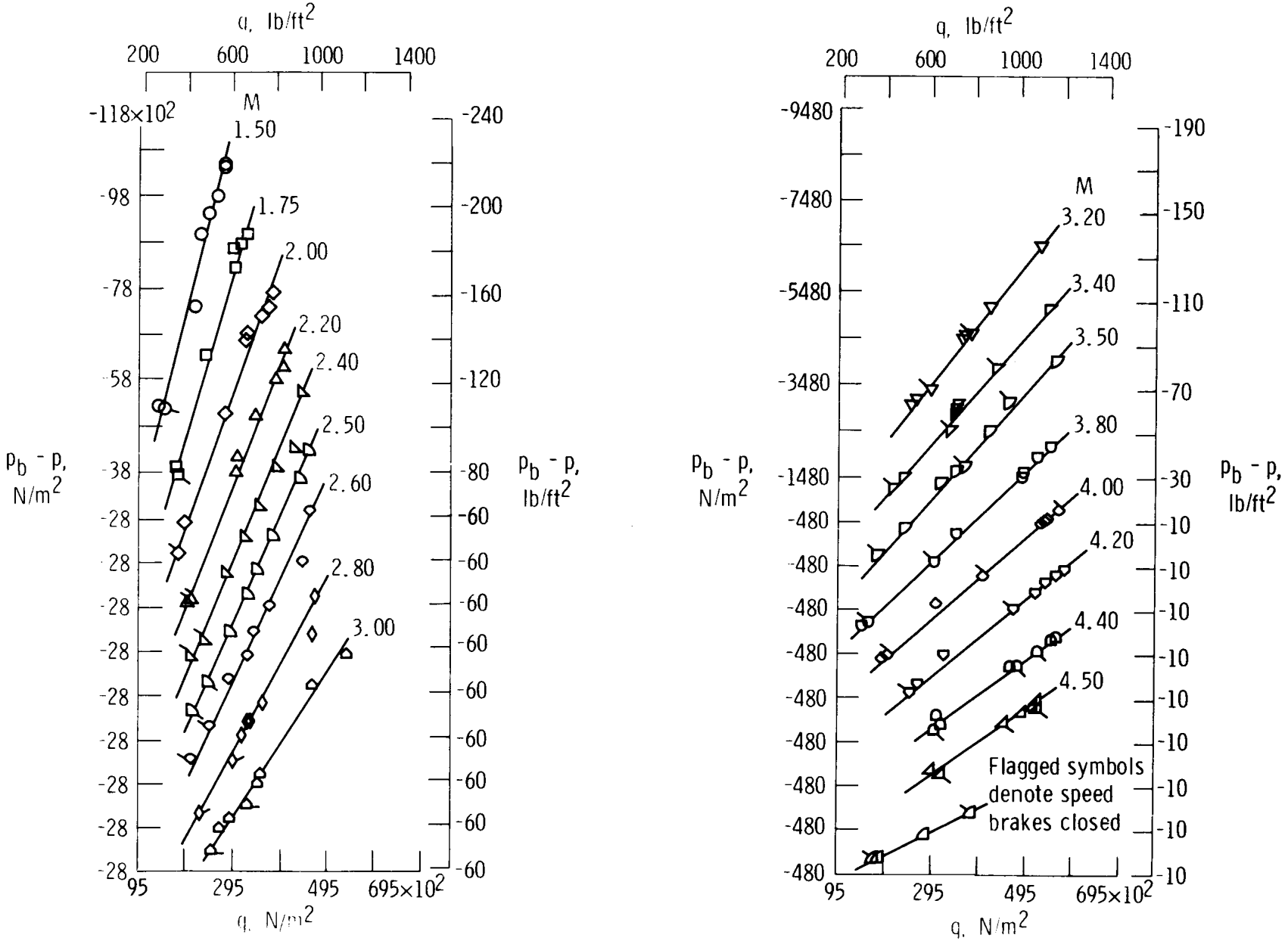

Figure 13. Difference between base pressure and free-stream pressure as a function of dynamic pressure for the X-15 flight data.

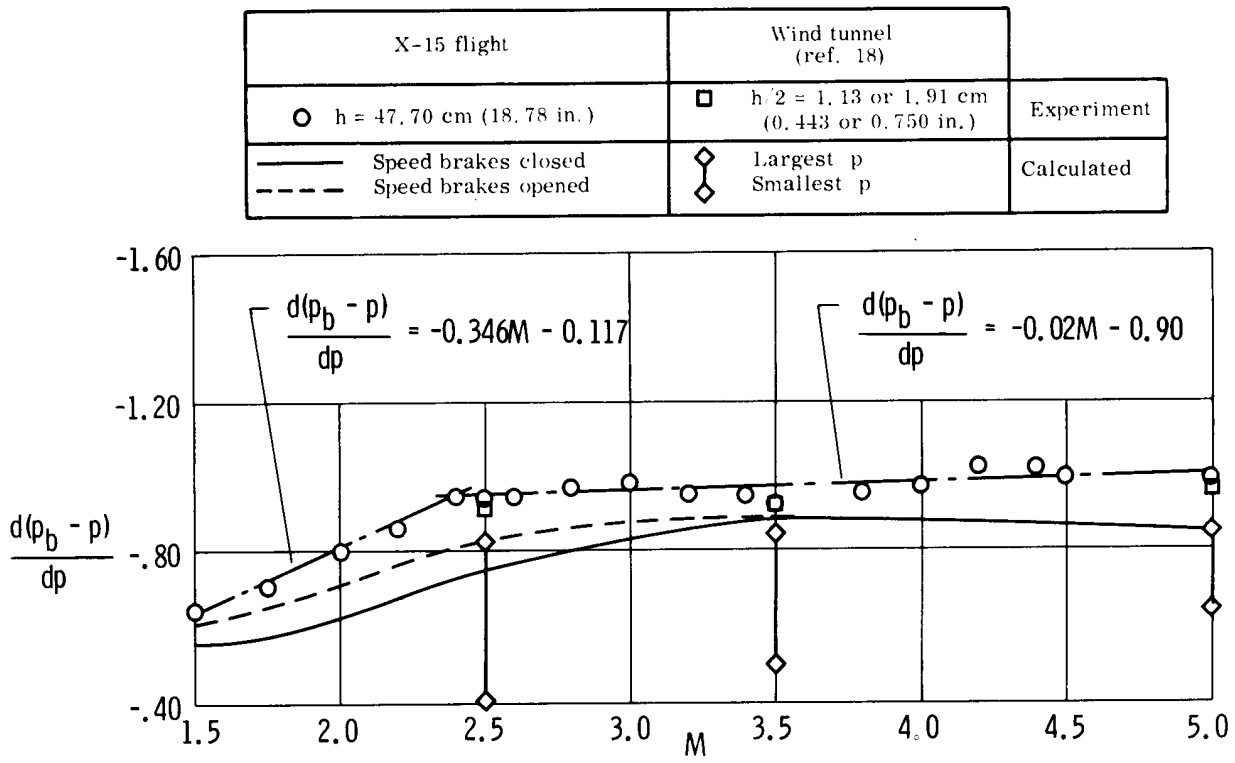

(a) Slopes from figure 12 and calculated from equation (1).

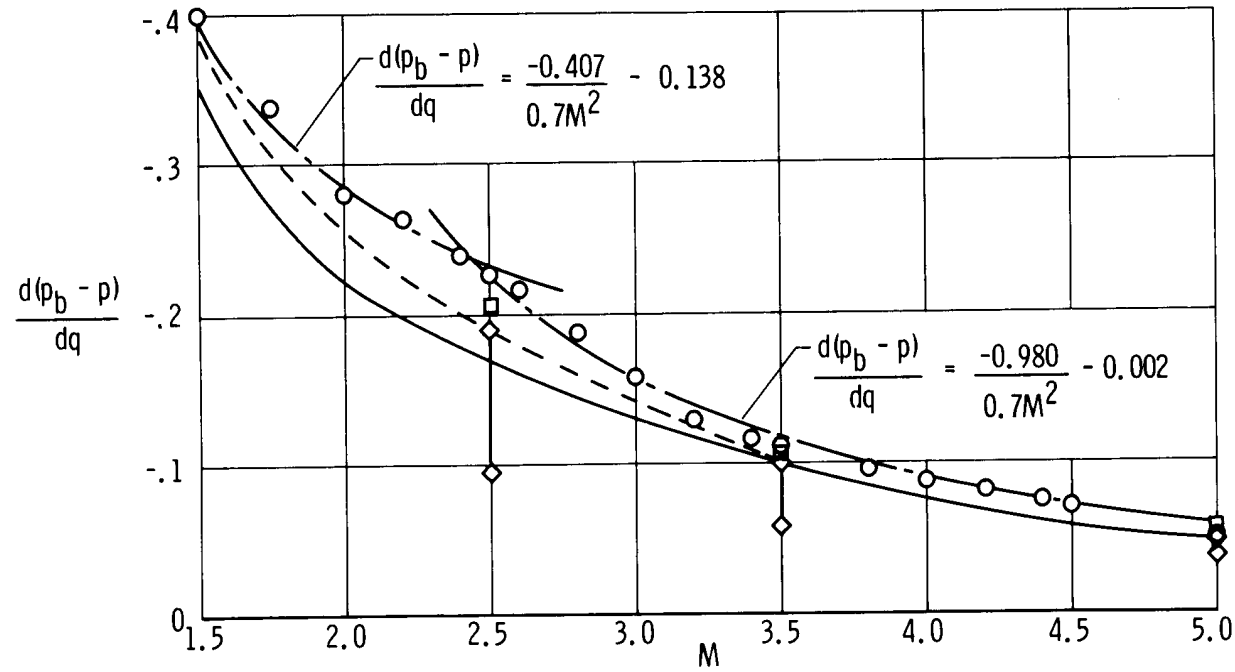

(b) Slopes from figure 13 and calculated from equation (2).

Figure 14. Variation of $\frac{d(p_b - p)}{dp}$ and $\frac{d(p_b - p)}{dq}$ with Mach number and comparison with calculated and empirical values.

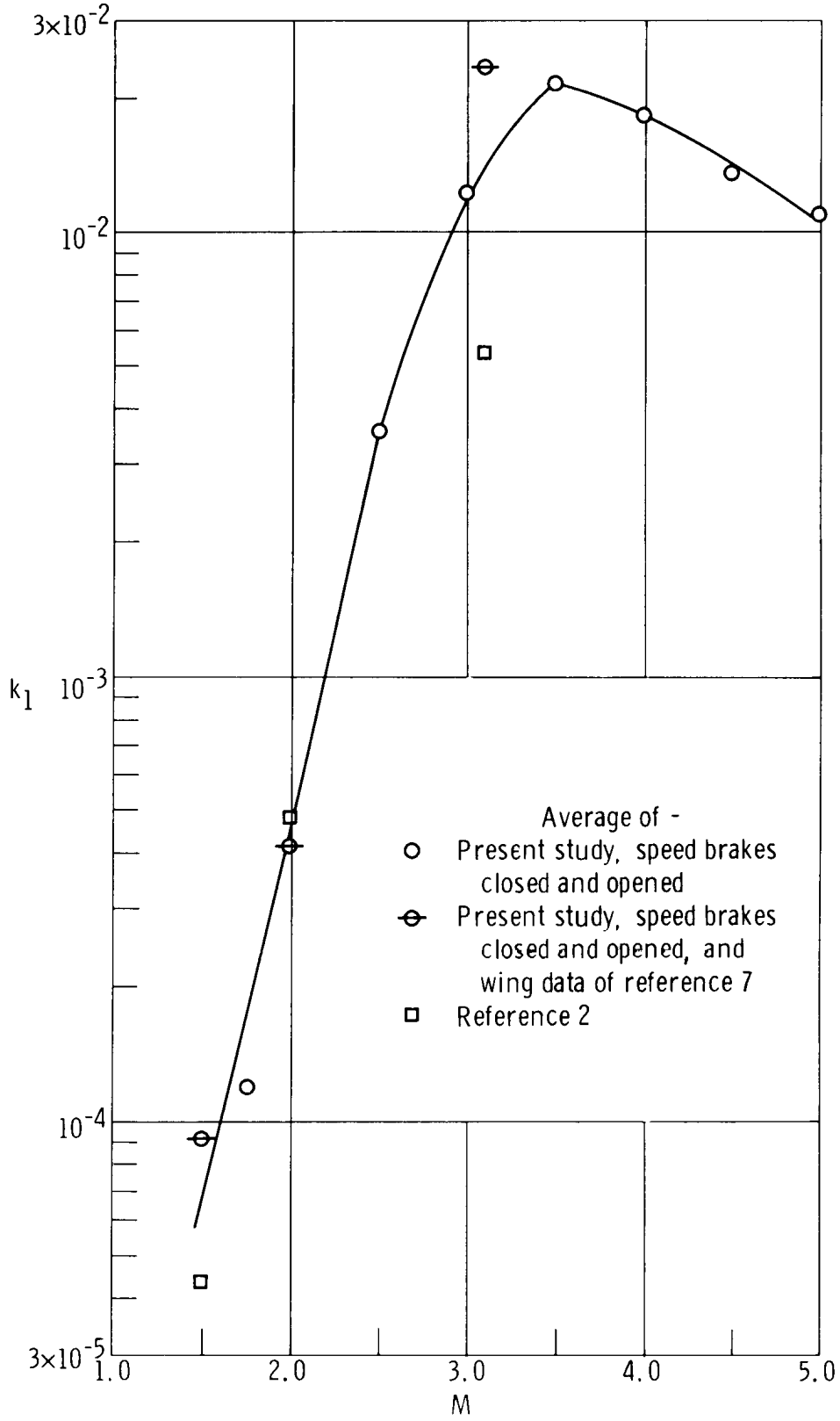

Figure 15. Mach-number-dependent value as a function of Mach number.

NASA-Langley, 1971 — 12 H-602